Supporting Information for

Lanthanide-Organic Pincer Hosts with Allosteric-Controlled Metal Ion Binding Specificity

Chen Jiang,[a,b] Shao-Jun Hu,[a,b] Li-Peng Zhou,[a] Jian Yang*[a] and Qing-Fu Sun*[a,b]

a. State Key Laboratory of Structural Chemistry, Fujian Institute of Research on the Structure of Matter, Chinese Academy of Sciences, Fuzhou 350002, People's Republic of China.

b. University of Chinese Academy of Sciences, Beijing 100049, People's Republic of China.

Cotents

1. General 1
2. Experimental details and characterization 2
3. NMR spectra 5
4. Photophysical properties 17
5. UV-vis titration spectra and the determination of binding constant 20
6. ESI-TOF-MS spectra 27
7. Single crystal X-ray diffraction studies 32
8. Reference 42

1. General

Unless otherwise stated, all chemicals and solvents were purchased from commercial companies and used without further purification. Deuterated solvents were purchased from Admas, J&K scientific and Sigma-Aldrich. 1D and 2D-NMR spectra were measured on a Bruker Biospin Avance III (400 MHz) spectrometer and JEOL ECZ600S (600 MHz) spectrometer. ^{1}H-NMR chemical shifts were determined with respect to TMS or residual signals of the deuterated solvents used. ESI-TOF-MS were recorded on an Impact II UHR-TOF mass spectrometry from Bruker, with tuning mix as the internal standard. Data analysis was conducted with the Bruker Data Analysis software (Version 4.3) and simulations were performed with the Bruker Isotope Pattern software. UV-Vis spectra are recorded on UV-2700 UV-Visible spectrophotometer from SHIMADZU. Excitation and emission spectra were recorded on the FS5 spectrofluorometer from Edinburg Photonics. Spectra were corrected for the experimental functions.

2. Experimental details and characterization

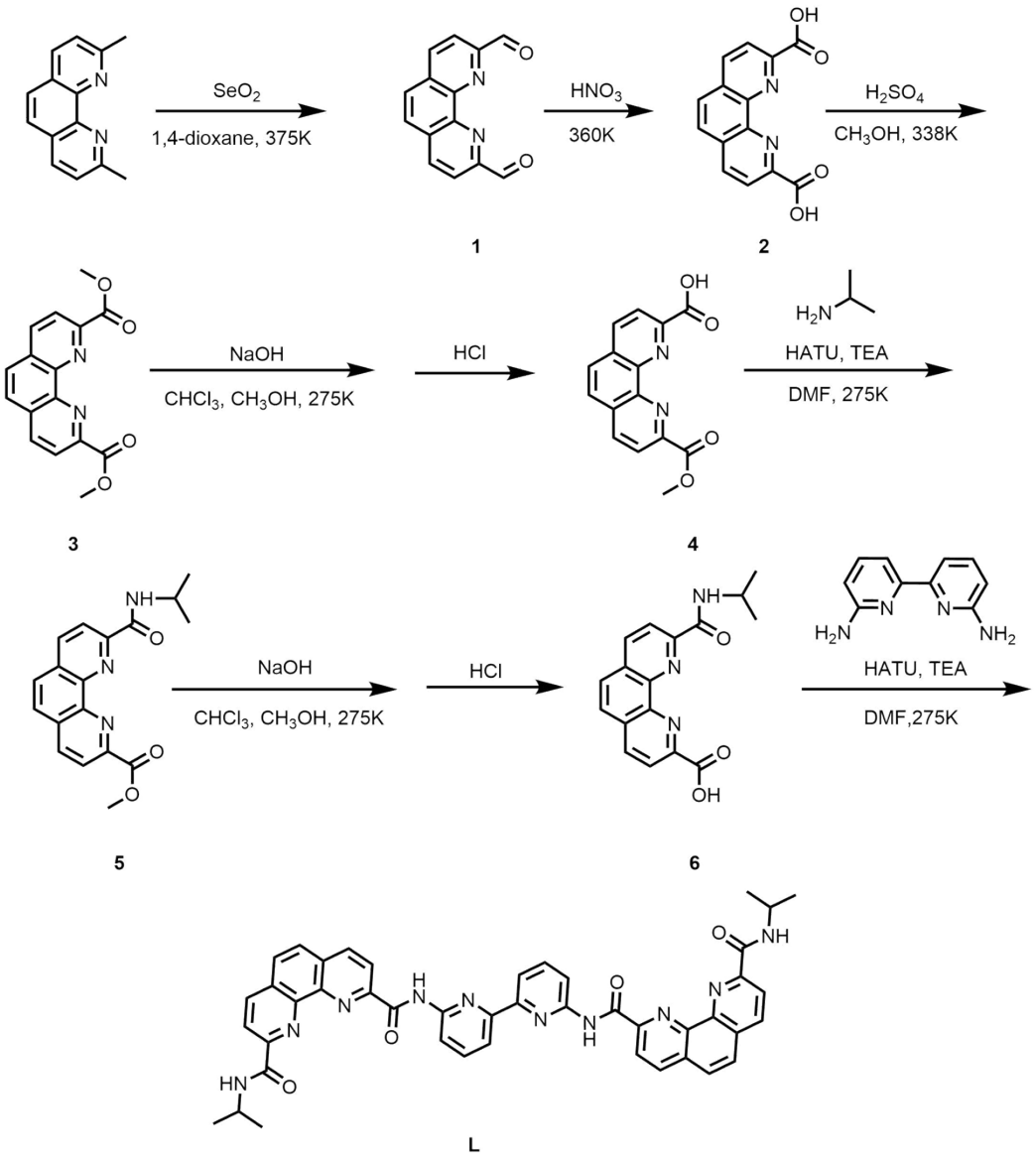

Scheme S1. Synthetic procedures of the ligand **L**

The preparation of compounds **1, 2** and **3** was synthesized following the literature procedure.[S1]

Synthesis of compound 4:

3 (850 mg, 2.87 mmol, 1.0 equiv) was added to a mixed solution of methanol and chloroform (v/v = 100 mL: 200 mL). NaOH (110 mg, 2.75 mmol, 0.96 equiv) was dissolved in in a mixed solvent of methanol and water (v/v =10 mL: 10 mL). Subsequently, the NaOH solution was added dropwise to the solution of **3** under ice-water bath condition. Then the solvent was removed under reduce pressure and the residue was extracted with dichloromethane and water. Finally, the aqueous phase was collected and neutralized by HCl (2 M), and the precipitate was collected by filtration and dried under vacuum oven. The product **4** was obtained as white powder (567 mg, 70%). ^{1}H NMR (600 MHz, DMSO-d_6, 298 K) δ (ppm): 8.74 (d, J = 7.8 Hz, 1H), 8.71 (d, J = 8.3

Hz, 1H), 8.42 – 8.39 (m, 2H), 8.19 (s, 2H), 3.99 (s, 3H). ^{13}C NMR (151 MHz, DMSO-d_6, 298 K): δ 166.97 (*C*O), 165.99 (*C*O), 149.09(*C*q), 147.92 (*C*q), 145.52 (*C*q), 145.37 (*C*q), 138.82 (*C*H), 138.70 (*C*H), 131.17 (*C*q), 131.00 (*C*q), 129.19 (*C*H), 128.88 (*C*H), 124.26 (*C*H), 124.09 (*C*H), 53.36 (*C*H$_3$). ESI-TOF-MS: calcd for $C_{15}H_{10}N_2O_4$, *m/z* 305.0540 $[M + Na^+]^+$; found: 305.0533.

Synthesis of compound 5-6:

4 (1.89 g, 6.67 mmol, 1.0 equiv), propan-2-amine (599 mg, 10.02 mmol, 1.5 equiv) and DMF (50 mL) were added into a 100 mL one-necked flask. After cooling down with ice water, HATU/2-(7-Aza-1H-Benzotriazole-1-yl)-1,1,3,3-tetramethyluronium hexafluorophosphate (5.07 g, 13.34 mmol, 2.0 equiv) and Et_3N (1 mL) were added, then the reaction mixture was stirred for 16 h. The solvent was removed under reduced pressure, and the crude product was extracted with dichloromethane and water. Then the organic phase was combined and the solvent was removed under reduced pressure and the crude material **5** was obtained as a white power (1.25 g, 58%). Then **5** (1.25 g, 3.87 mmol, 1.0 equiv) was added to a mixed solution of methanol and chloroform (v/v = 100 mL: 200 mL), NaOH (148 mg, 3.72 mmol, 0.96 equiv) was dissolved in in a mixed solvent of methanol and water (v/v = 10 mL :10 mL). Subsequently, the NaOH solution was added dropwise to the solution of **5** under ice-water bath. Then the solvent was removed under reduce pressure, and the rotary evaporated product was extracted with dichloromethane and water. Finally, the aqueous phase was collected, and neutralized by HCl (2M). The precipitate was collected by filtration. After that, the product **6** was obtained as white powder (952 mg, 79%). ^{1}H NMR (400 MHz, DMSO-d_6, 298 K) δ (ppm): 9.41 (d, J = 8.0 Hz, 1H), 8.77-8.73 (m, 2H), 8.45 (dd, J = 8.5, 2.0 Hz, 2H), 8.23 – 8.17 (m, 2H), 4.27 – 4.19 (m, 1H), 1.31 (d, J = 6.6 Hz, 6H). ^{13}C NMR (151 MHz, DMSO-d_6, 298 K): δ 171.28 (*C*O), 168.18 (*C*O), 154.99 (*C*q), 153.17 (*C*q), 149.50 (*C*q), 148.99 (*C*q), 143.59 (*C*H), 143.41 (*C*H), 135.76 (*C*q), 135.45 (*C*q), 133.77 (*C*H), 133.03 (*C*H), 128.55 (*C*H), 126.22 (*C*H), 46.41 (*C*H). 27.61 (*C*H$_3$). ESI-TOF-MS: calcd for $C_{17}H_{15}N_3O_3$, *m/z* 310.1152 $[M + H^+]^+$; found: 310.1186.

Synthesis of L:

6 (380 mg, 1.23 mmol, 2.2 equiv), [2,2'-bipyridine]-6,6'-diamine (104 mg, 0.559 mmol, 1 equiv) and DMF (50 mL) were added into a 100 mL one-necked flask. After cooling down with ice bath, HATU/2-(7-aza-1H-benzotriazole-1-yl)-1,1,3,3-tetramethyluronium (425 mg, 1.18 mmol, 2.0 equiv) and Et_3N (1 mL) were added, then the reaction mixture was stirred for 16 h. The solvent was removed under reduced pressure, and the crude product was extracted with dichloromethane and water. The organic phases were then combined, the solvent was removed under reduced pressure, and the crude product was isolated and purified by column chromatography (SiO_2, DCM/MeOH = 200: 3) to give **L** as a pale yellow solid. (185 mg, 43.3%). ^{1}H NMR (400 MHz, $CDCl_3$, 298 K) δ (ppm): 10.95 (s, 1H), 8.74 (d, J = 8.4 Hz, 1H), 8.65 – 8.60 (m, 3H), 8.55 (d, J = 8.0 Hz, 1H), 8.48 (d, J = 8.4 Hz, 1H), 8.15 (d, J = 7.5 Hz, 1H), 7.99 – 7.94 (m, 3H), 4.34 – 4.29 (m, 1H), 1.28 (d, J = 6.6 Hz, 6H). ^{13}C NMR (151 MHz, $CDCl_3$, 298 K): δ 163.42 (*C*O), 163.12 (*C*O), 155.05 (*C*q), 150.98 (*C*q), 150.42 (*C*q), 149.49 (*C*q), 144.52 (*C*q), 144.32 (*C*q), 139.18 (*C*H), 138.29 (*C*H), 137.96 (*C*H), 131.03 (*C*H), 130.69 (*C*q), 128.52 (*C*H), 127.70 (*C*H), 121.86 (*C*H), 121.84 (*C*H), 118.44 (*C*H), 114.72 (*C*H), 39.07 (*C*H), 19.86 (*C*H$_3$). ESI-TOF-MS: calcd for $C_{44}H_{36}N_{10}O_4$, m/z 791.2392 $[M + H^+]^+$; found: 791.2831.

Synthesis of LaL(OTf)$_3$:

To a yellow suspension of **L** (1.87 mg, 2.43 μmol) in 500 μL mixed solvent of acetonitrile and methanol (v/v = 4: 1) was added La(OTf)$_3$ (1.65 mg, 2.43 μmol), and then the mixture was stirred at 50 °C for 2 h. The turbid suspension gradually turned into a homogenous yellow solution. ^{1}H NMR showed quantitative formation of La**L**(OTf)$_3$. ^{1}H NMR (400 MHz, Methanol-d_4, 298 K) δ (ppm): 9.12 (dd, J = 20.1, 8.4 Hz, 1H), 8.98 (dd, J = 8.4, 1.5 Hz, 1H), 8.84 (dd, J = 8.5, 5.7 Hz, 1H), 8.46 – 8.32 (m, 2H), 8.30 – 8.18 (m, 3H), 7.76 – 7.69 (m, 1H), 2.43 – 2.39 (m, 1H), 0.71 (d, J = 6.6 Hz, 3H), 0.38 (dd, J = 14.3, 6.7 Hz, 3H). ^{13}C NMR (151 MHz, Methanol-d_4, 298 K) δ 158.34 (*C*O), 156.43 (*C*O), 152.09 (*C*q), 150.87 (*C*q), 149.09 (*C*H), 147.54 (*C*q), 146.71 (*C*q), 146.21 (*C*H), 144.45 (*C*H), 142.50 (*C*H), 132.77 (*C*q), 130.73 (*C*q), 130.25 (*C*q), 129.26 (*C*H), 126.90 (*C*q), 122.97 (*C*H), 122.59 (*C*H), 120.97 (*C*H), 117.50 (*C*H), 45.07 (*C*H), 21.66 (*C*H$_3$), 21.51 (*C*H$_3$). ESI-TOF-MS for La($C_{44}H_{36}N_{10}O_4$)(CF_3SO_3)$_3$: calcd for $[M - (CF_3SO_3^-)]^+$ 1205.0907, found 1205.0920; calcd for $[M - 2(CF_3SO_3^-)]^{2+}$ 528.0691, found 528.0706.

Synthesis of EuL(OTf)$_3$:

Complex Eu**L** was synthesized as the same procedure as **LaL**, starting from Eu(OTf)$_3$. ^{1}H NMR showed quantitative formation of Eu**L**(OTf)$_3$. ^{1}H NMR (400 MHz, Methanol-d_4, 298 K) δ (ppm): 9.87 (t, J = 8.0 Hz, 1H), 9.66 (d, J = 7.9 Hz, 1H), 9.43 (t, J = 8.1 Hz, 1H), 9.31 (d, J = 7.9 Hz, 1H), 8.92 (s, 1H), 8.71 (s, 1H), 8.14 (s, 1H), 7.76 (s, 1H), 7.37 (s, 1H), 7.21 (s, 1H), 3.52 (d, J = 5.8 Hz, 1H), 2.47 (s, 3H), 0.88 (s, 3H). ESI-TOF-MS for Eu($C_{44}H_{36}N_{10}O_4$)(CF_3SO_3)$_3$: calcd for $[M - (CF_3SO_3^-)]^+$ 1219.1058, found 1219.1085; Calcd for $[M - 2(CF_3SO_3^-)]^{2+}$ 535.0767, found 535.0788.

Synthesis of LuL(OTf)$_3$:

Complex Lu**L** was synthesized as the same procedure as La**L**, starting from Lu(OTf)$_3$. ^{1}H NMR showed quantitative formation of Lu**L**(OTf)$_3$. ^{1}H NMR (400 MHz, Methanol-d_4, 298 K) δ (ppm): 10.41 (d, J = 8.5 Hz, 1H), 10.32 (d, J = 8.1 Hz, 1H), 10.08 (d, J = 8.5 Hz, 1H), 9.88 (d, J = 8.3 Hz, 1H), 9.72 (q, J = 9.1 Hz, 2H), 9.21 (t, J = 8.1 Hz, 1H), 9.09 (s, 1H), 8.74 (d, J = 7.4 Hz, 1H), 8.28 (d, J = 8.7 Hz, 1H), 5.95 (p, J = 6.7 Hz, 1H), 2.81 (d, J = 6.6 Hz, 6H). ^{13}C NMR (151 MHz, Methanol-d_4, 298 K) δ 172.06 (*C*O), 169.23 (*C*O), 157.88 (*C*q), 152.77 (*C*q), 148.24 (*C*q), 144.59 (*C*H), 143.88 (*C*H), 143.69 (*C*q), 142.72 (*C*H), 132.69 (*C*q), 132.52 (*C*q), 132.42 (*C*q), 130.46 (*C*H), 129.10 (*C*H), 125.11 (*C*H), 123.00 (*C*q), 120.88 (*C*H), 113.73 (*C*H), 111.17 (*C*H), 43.27 (*C*H), 22.05 (*C*H$_3$), 21.27 (*C*H$_3$). ESI-TOF-MS for Lu($C_{44}H_{36}N_{10}O_4$)(CF_3SO_3)$_3$: calcd for $[M - (CF_3SO_3^-)]^+$ 1109.1871, found 1109.1745; calcd for $[M - 2(CF_3SO_3^-)]^{2+}$ 480.1173, found 480.1131.

3. NMR spectra

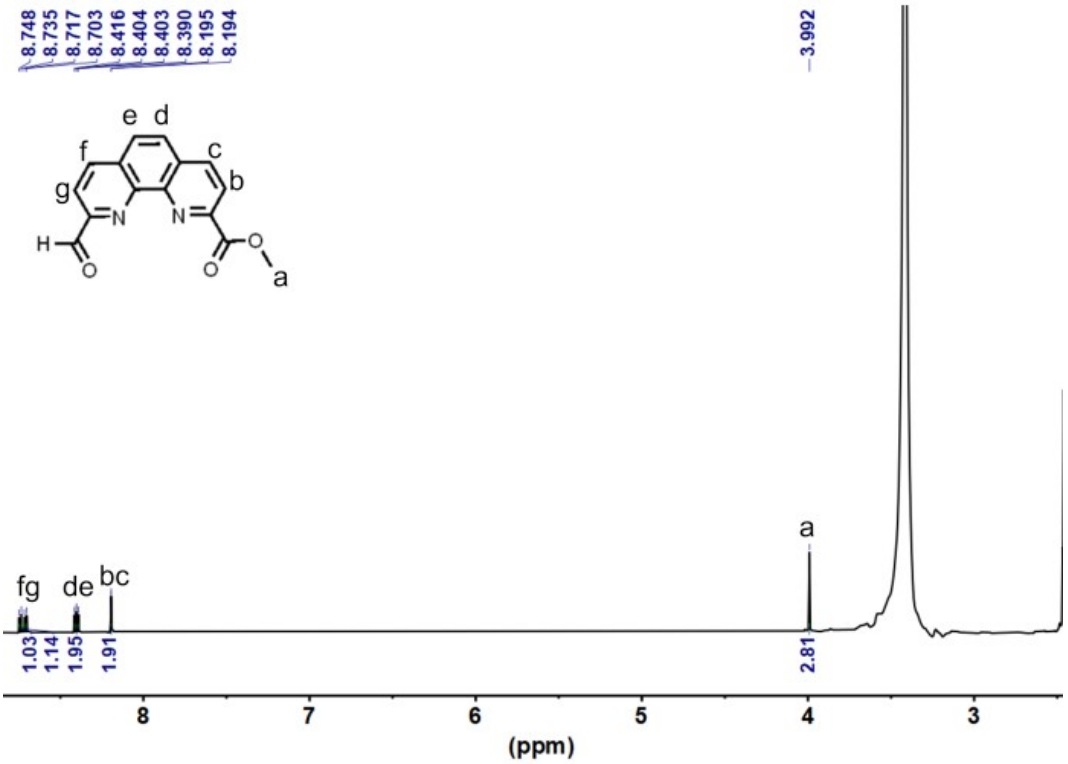

Figure S1. The ^{1}H NMR spectrum of **4** (600 MHz, DMSO-d_6, 298 K).

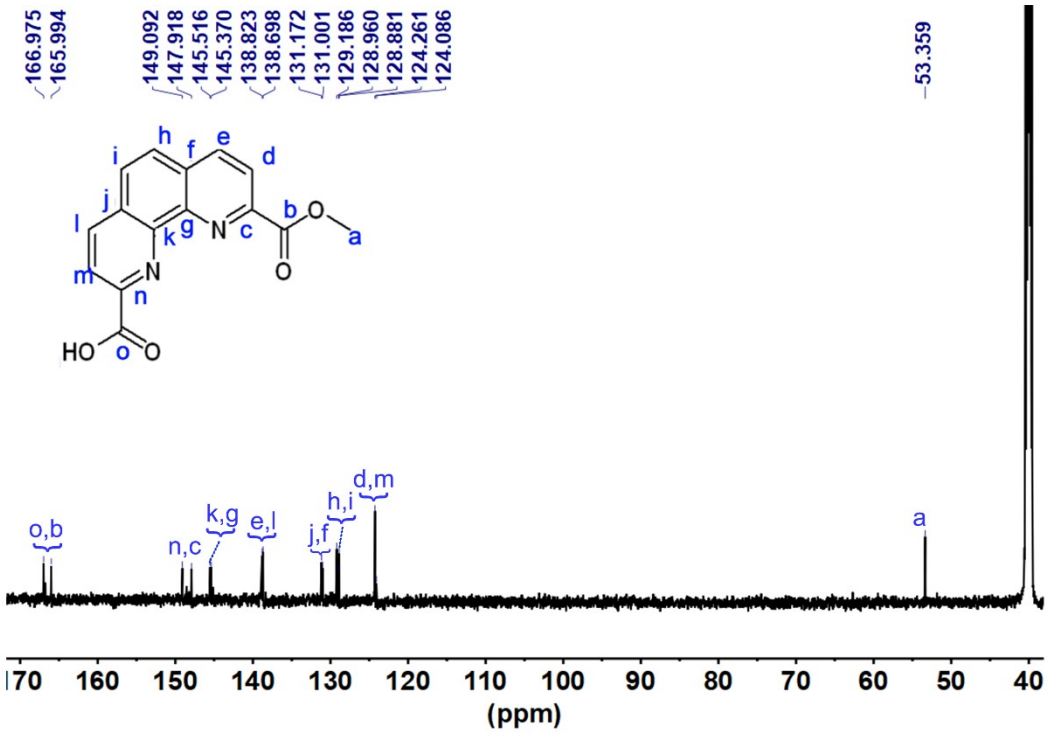

Figure S2. The ^{13}C NMR spectrum of **4** (151 MHz, DMSO-d_6, 298 K).

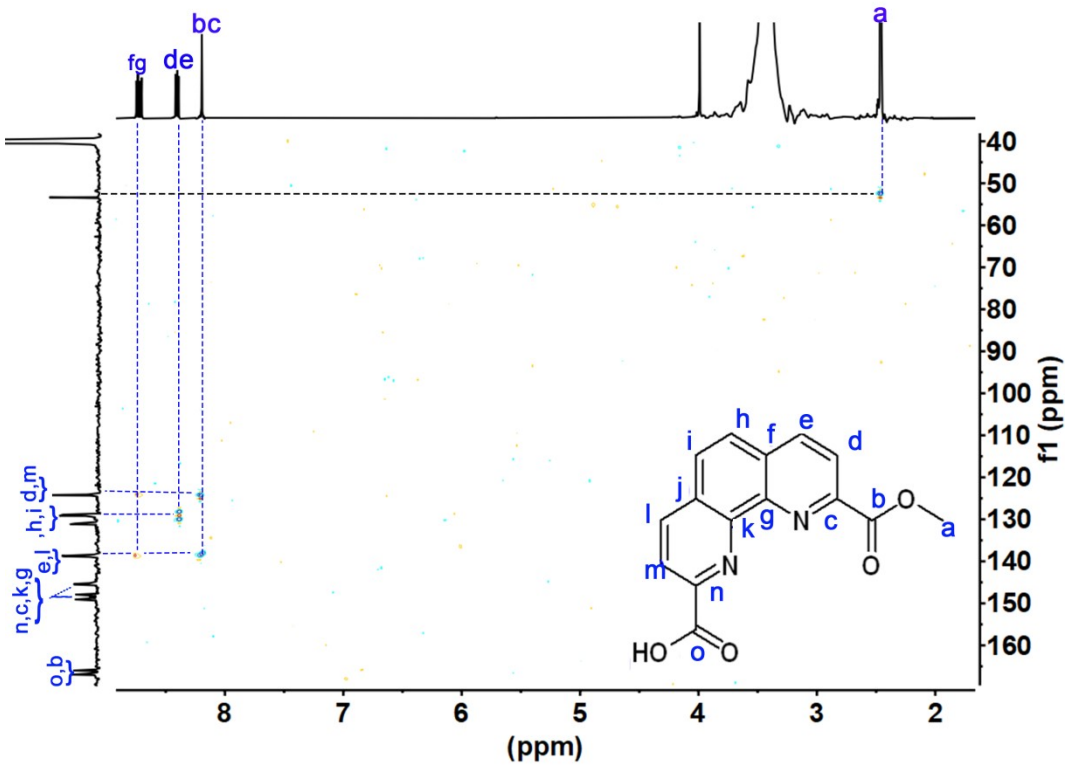

Figure S3. ^{1}H-{^{13}C} HSQC spectrum of **4** (600 MHz, DMSO-d_6, 298 K).

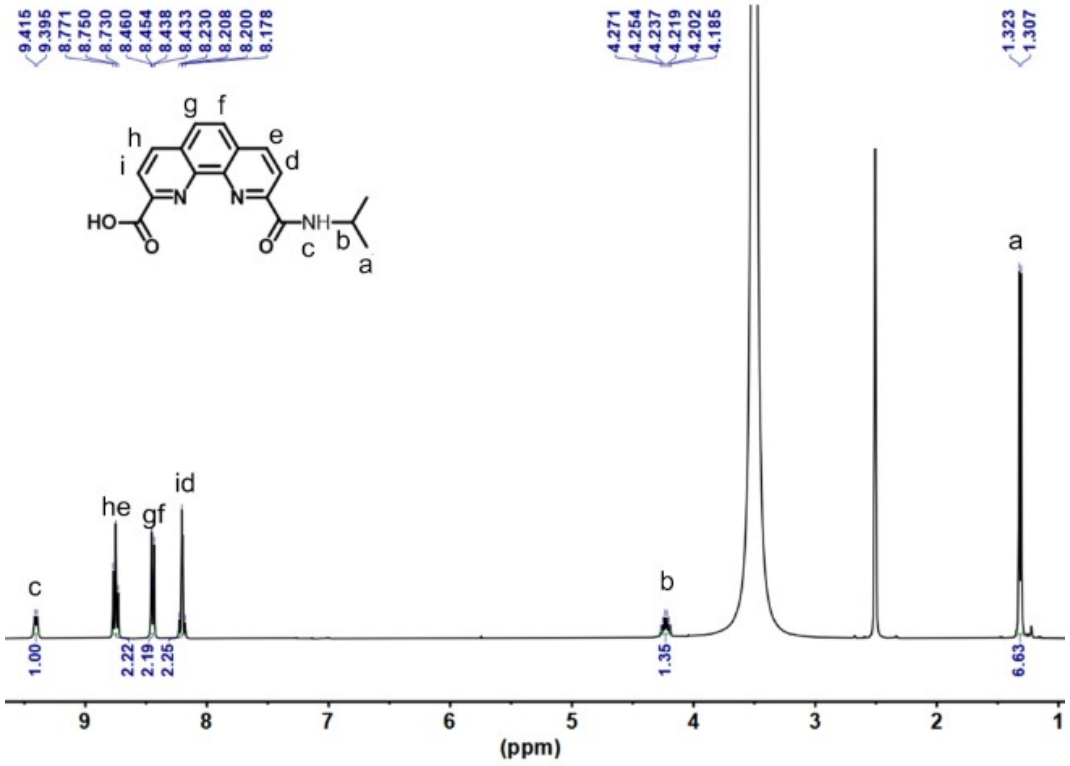

Figure S4. The ^{1}H NMR spectrum of **6** (400 MHz, DMSO-d_6, 298 K).

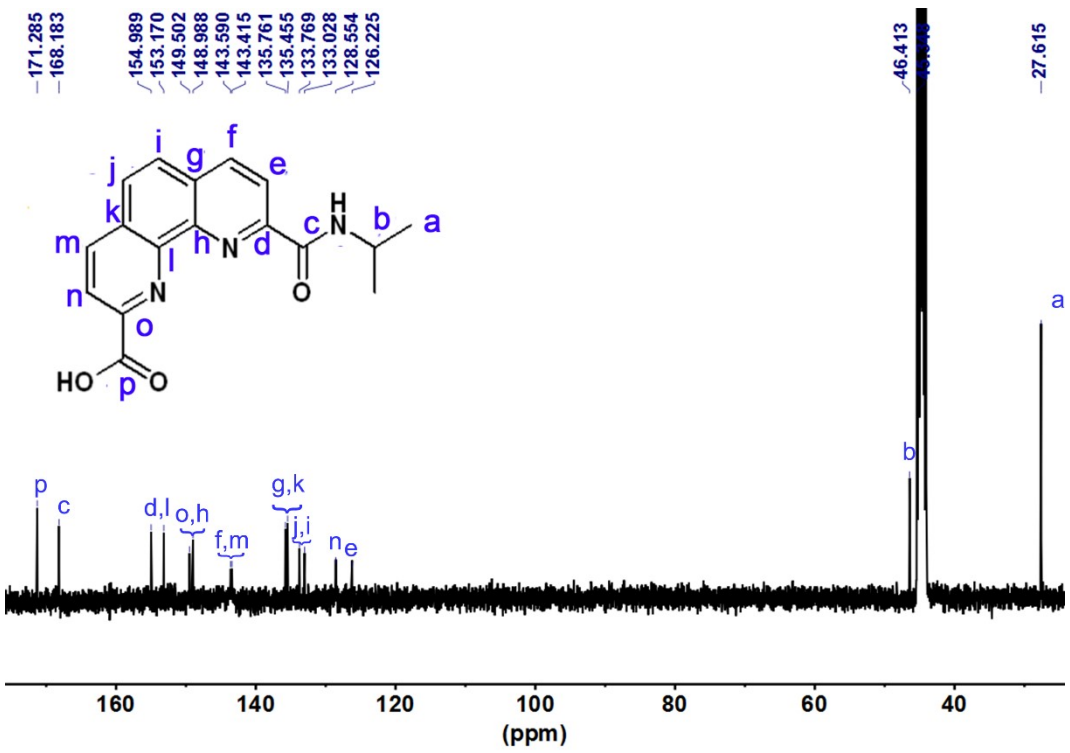

Figure S5. The ^{13}C NMR spectrum of **6** (151 MHz, DMSO-d_6, 298 K).

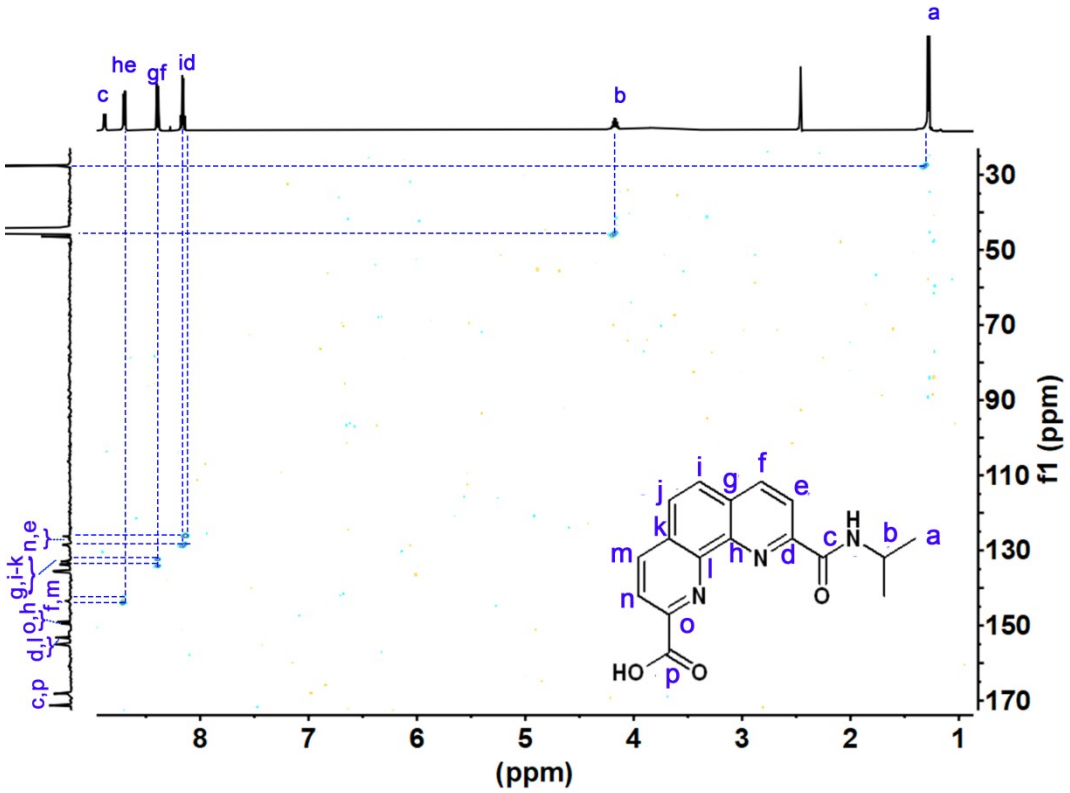

Figure S6. ^{1}H-{^{13}C} HSQC spectrum of **6** (600 MHz, DMSO-d_6, 298 K).

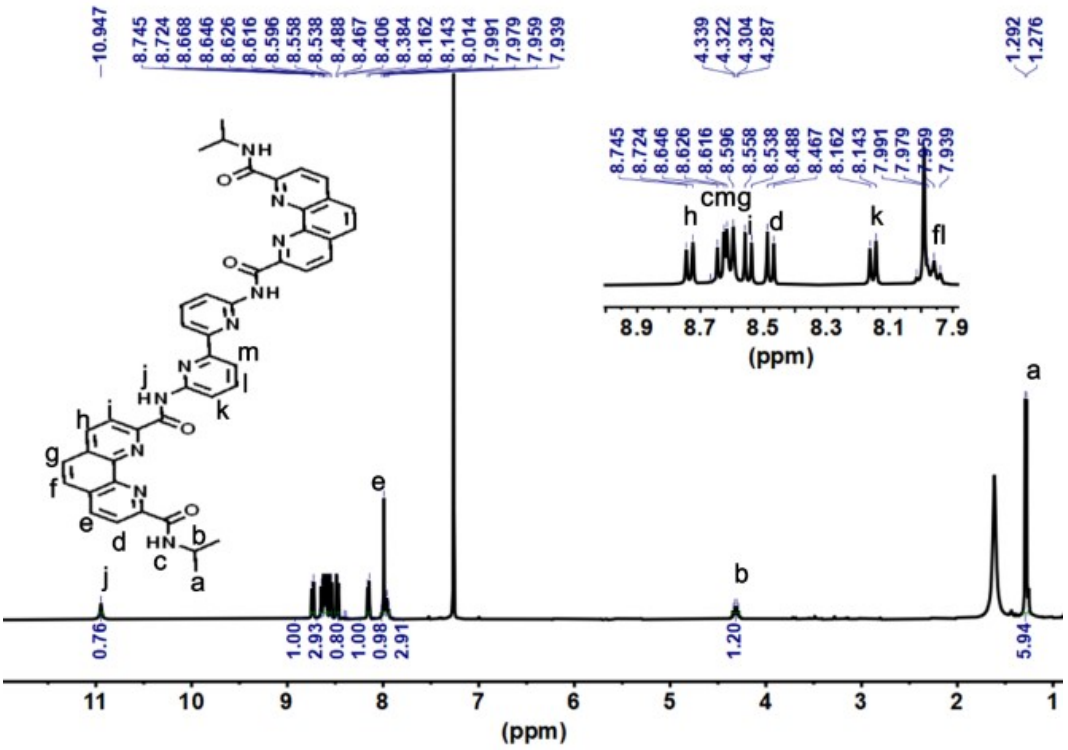

Figure S7. The ^{1}H NMR spectrum of **L** (400 MHz, $CDCl_3$, 298 K).

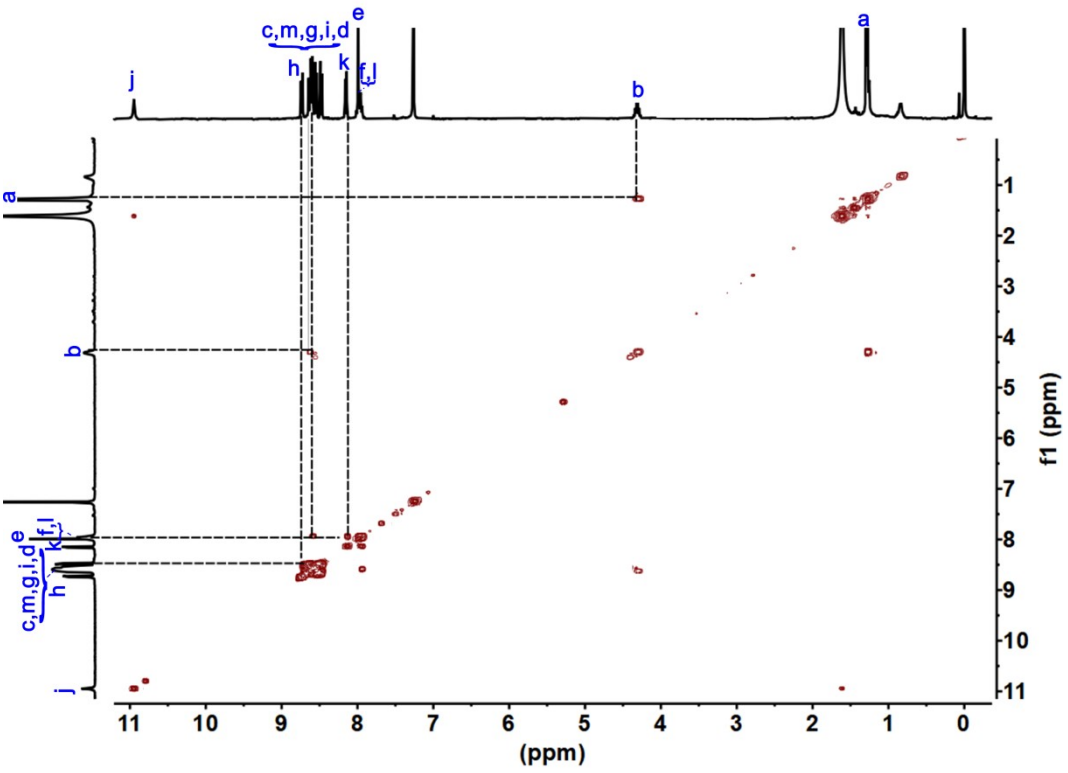

Figure S8. ^{1}H-^{1}H COSY NMR spectrum of **L** (400 MHz, $CDCl_3$, 298 K).

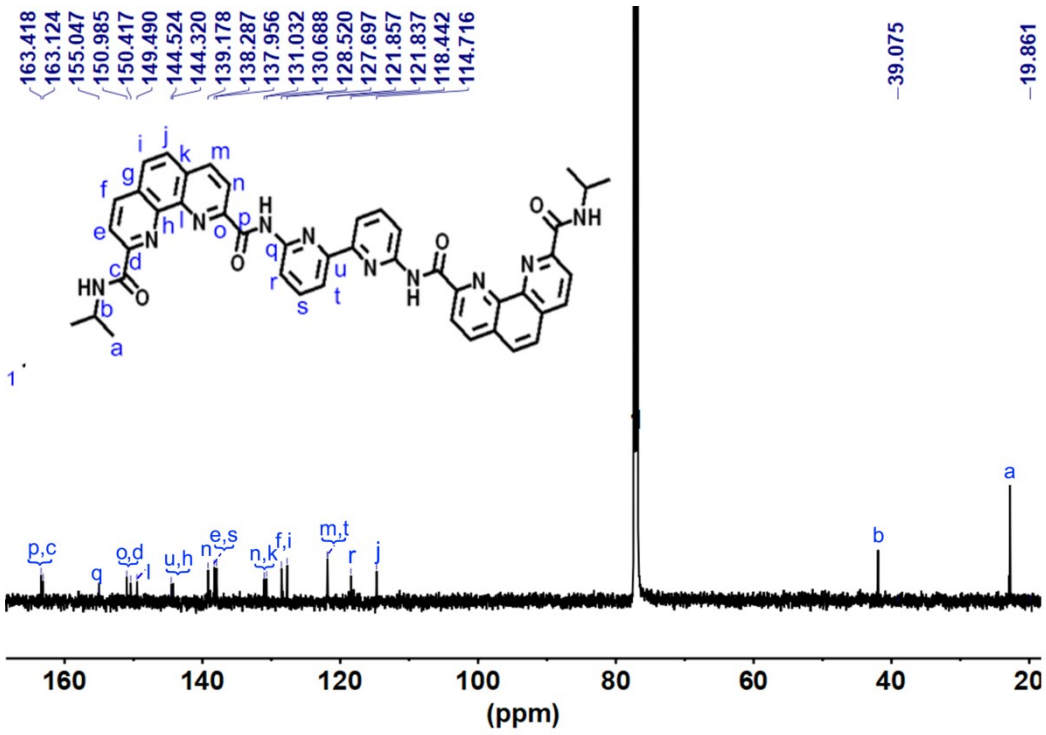

Figure S9. The ^{13}C NMR spectrum of **L** (151 MHz, $CDCl_3$, 298 K).

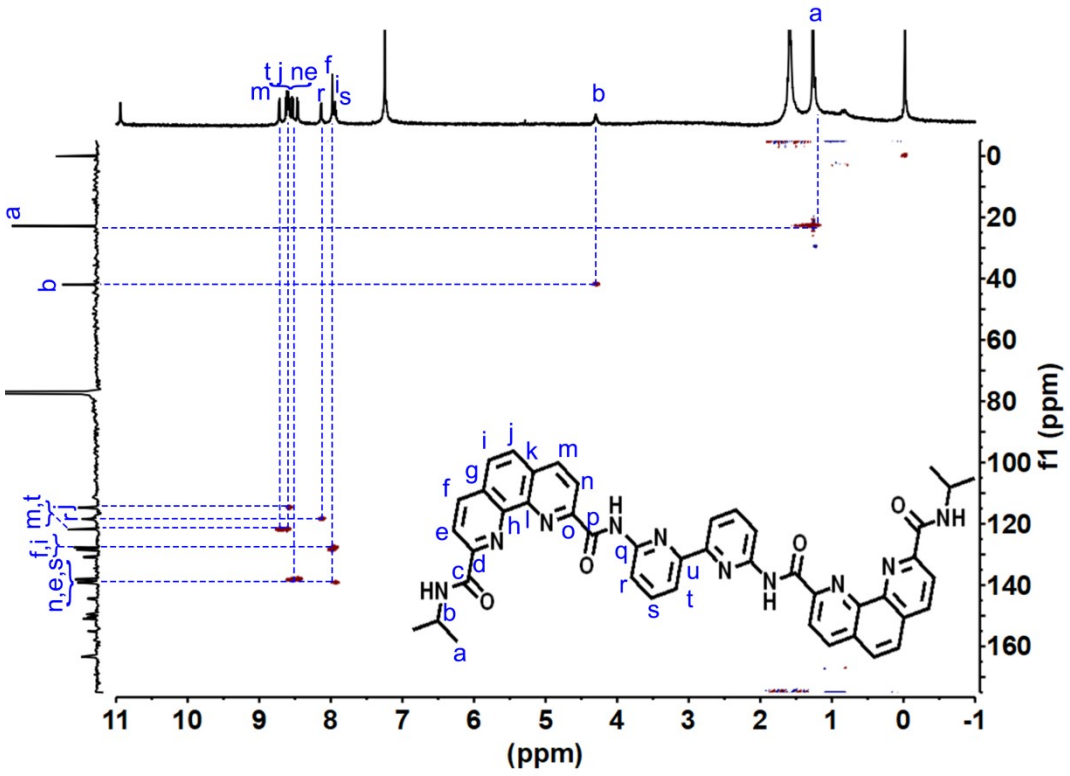

Figure S10. ^{1}H-{^{13}C} HSQC spectrum of **L** (600 MHz, $CDCl_3$, 298 K).

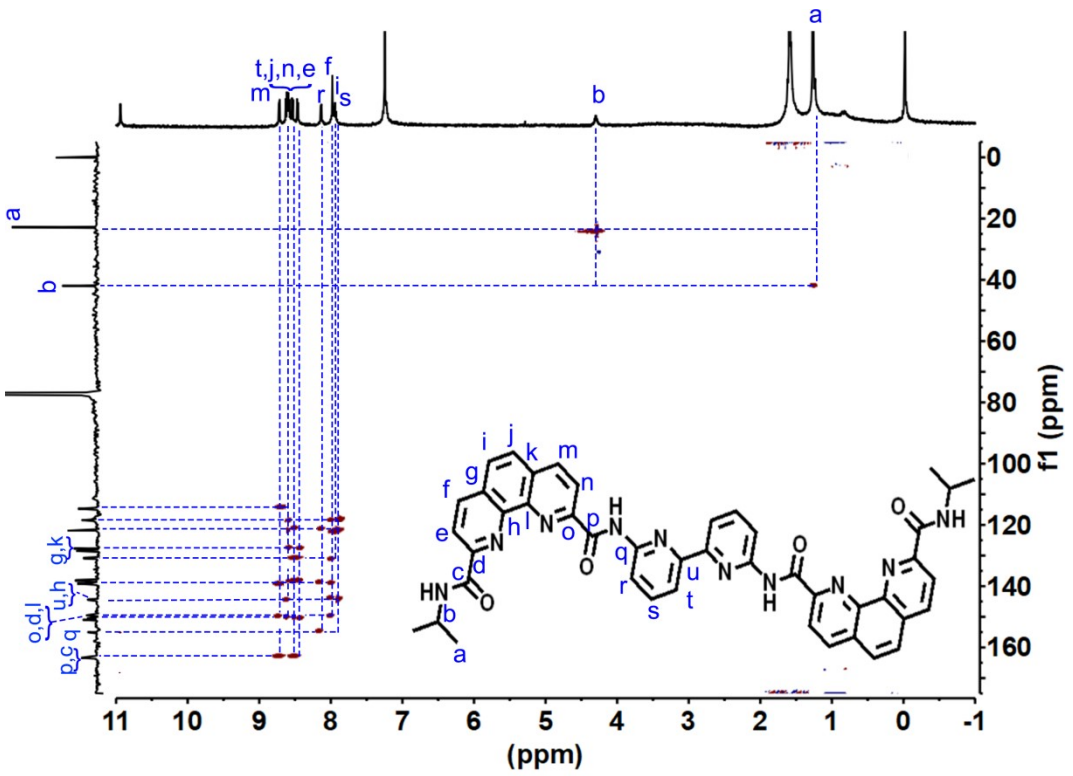

Figure S11. ^{1}H-{^{13}C} HMBC spectrum of **L** (600 MHz, $CDCl_3$, 298 K).

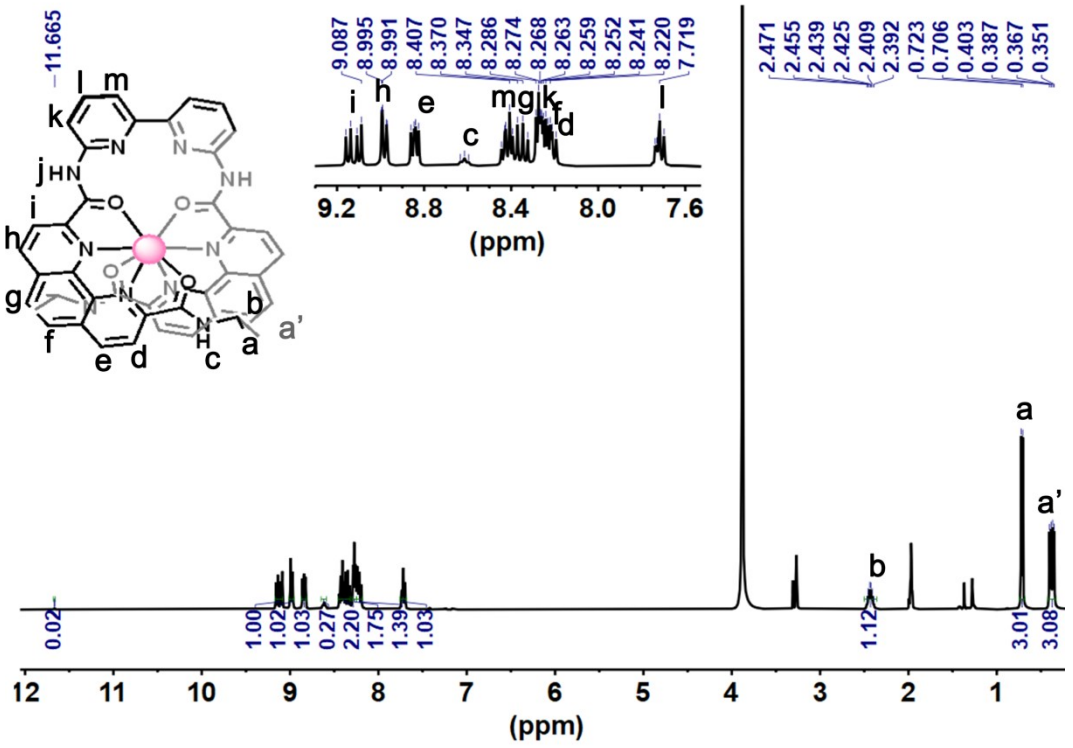

Figure S12. ^{1}H NMR spectrum of complex **LaL(OTf)$_3$** (400 MHz, CD_3CN/CD_3OD v/v = 4/1, 298 K).

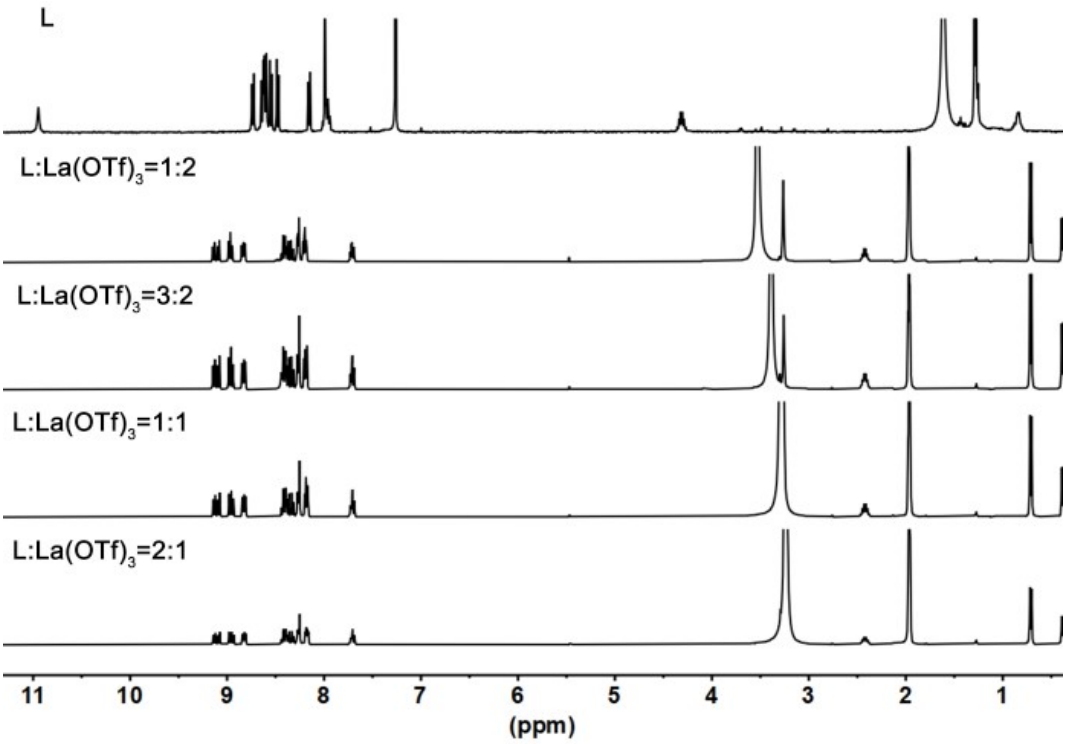

Figure S13. ^{1}H NMR spectra of self-assembly of **L** and La(OTf)$_3$ with changed ratio of **L**/La(OTf)$_3$ (400 MHz, CD_3CN/CD_3OD v/v = 4/1, 298 K).

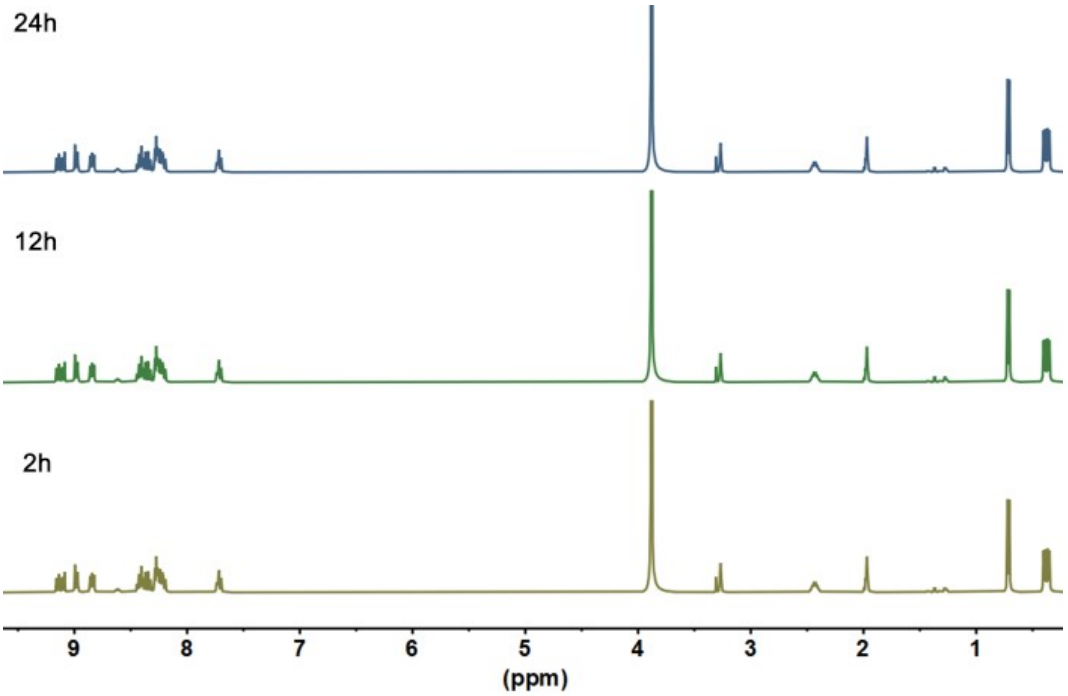

Figure S14. ^{1}H NMR spectra of L with La(OTf)$_3$ with different reaction time (400 MHz, CD_3CN/CD_3OD v/v = 4/1, 298 K).

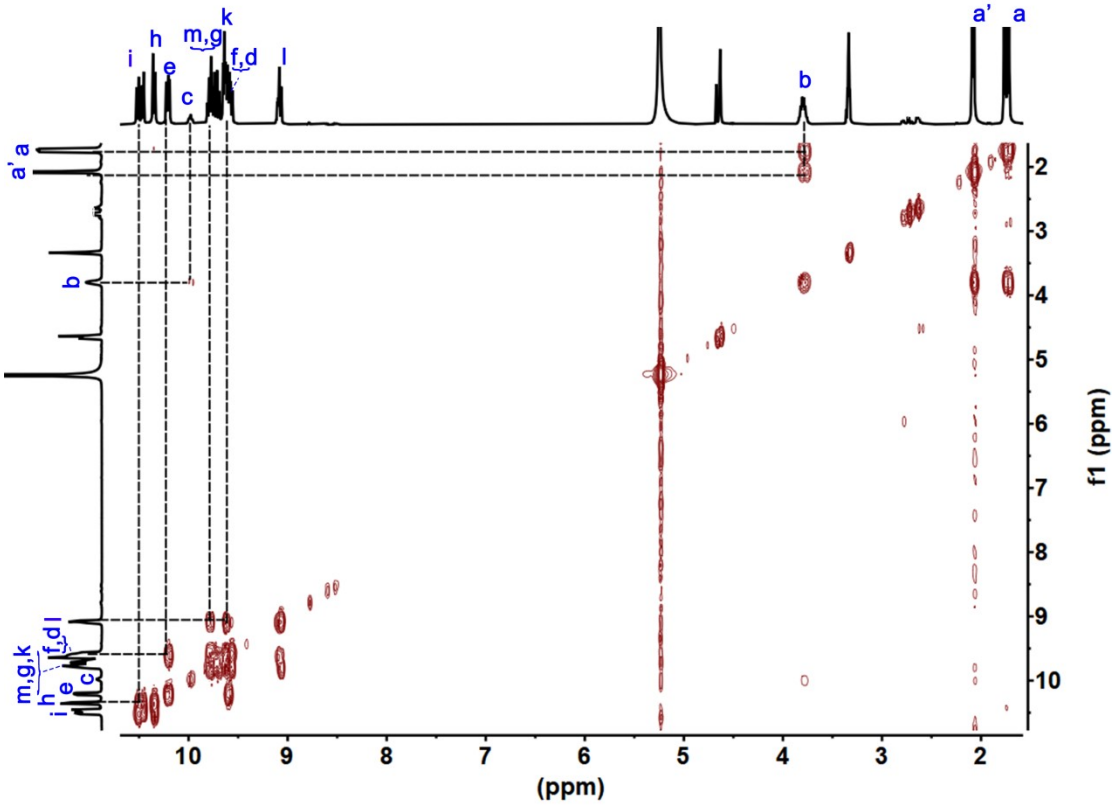

Figure S15. ^{1}H-^{1}H COSY NMR spectrum of complex **LaL(OTf)$_3$** (400 MHz, CD_3CN/CD_3OD v/v = 4/1, 298 K).

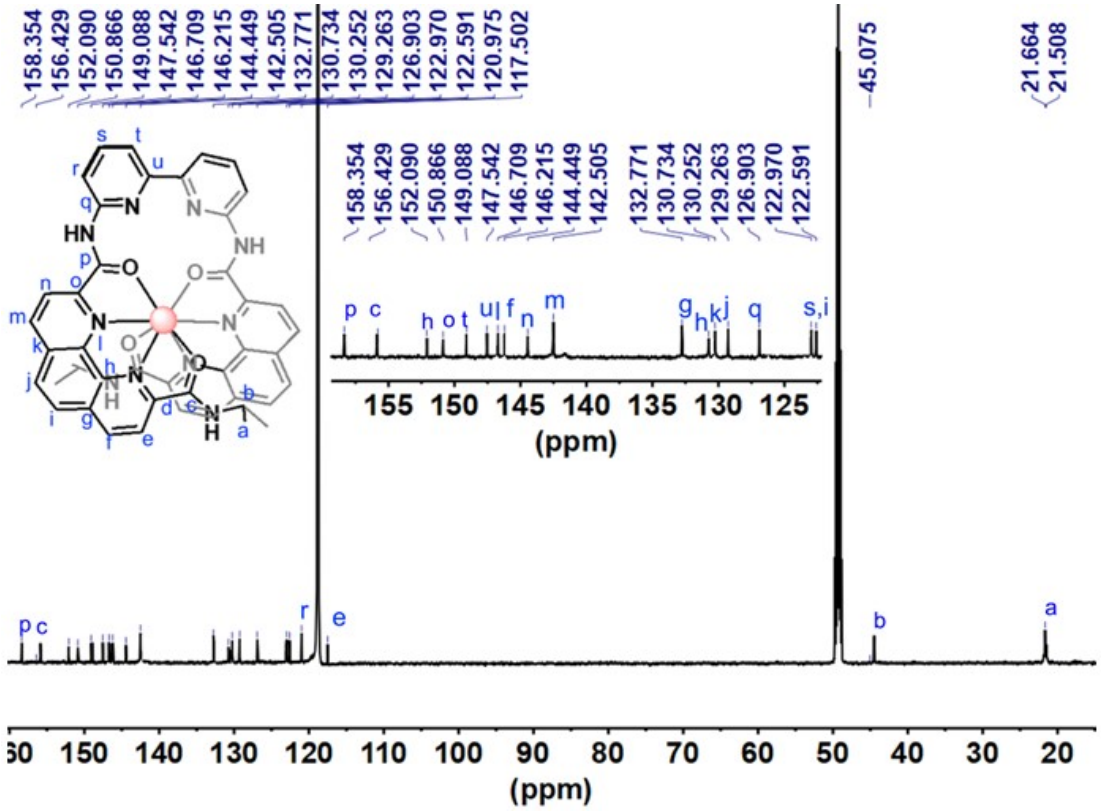

Figure S16. ^{13}C NMR spectrum of complex **LaL(OTf)$_3$** (151 MHz, CD_3CN/CD_3OD v/v = 4/1,

298 K).

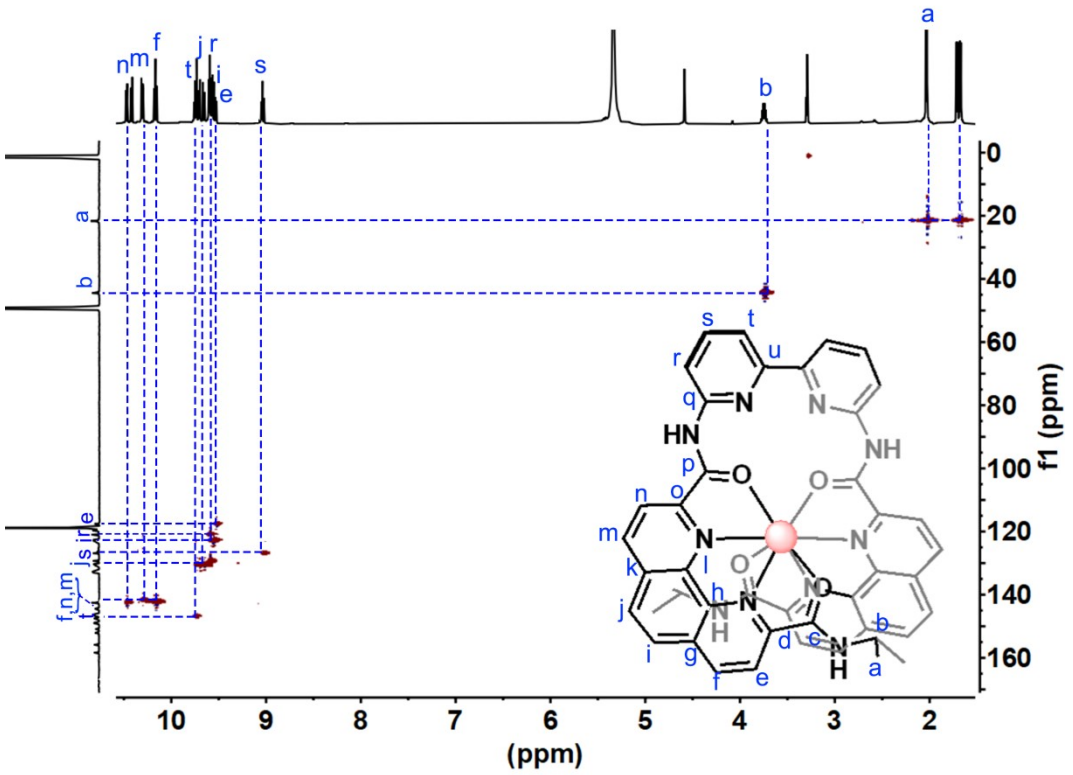

Figure S17. ^{1}H-{^{13}C} HSQC spectrum of **LaL(OTf)$_3$** (600 MHz, CD_3CN/CD_3OD v/v = 4/1, 298 K).

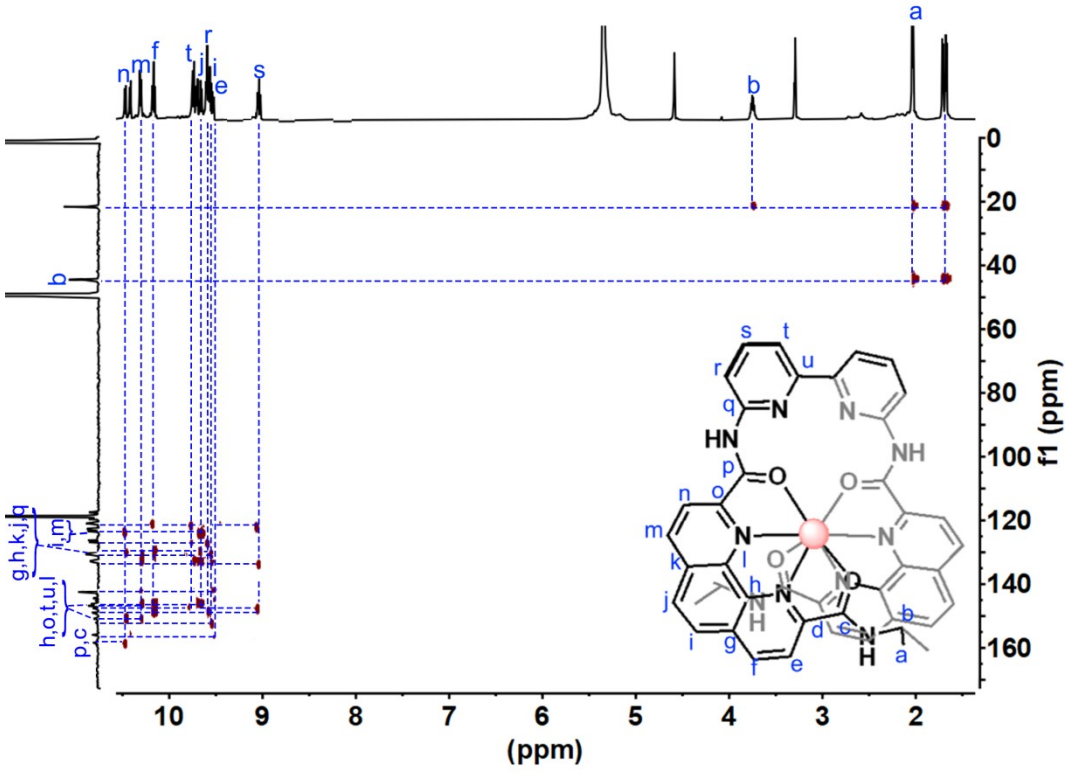

Figure S18. ^{1}H-{^{13}C} HMBC spectrum of **LaL(OTf)$_3$** (600 MHz, CD_3CN/CD_3OD v/v = 4/1, 298

K).

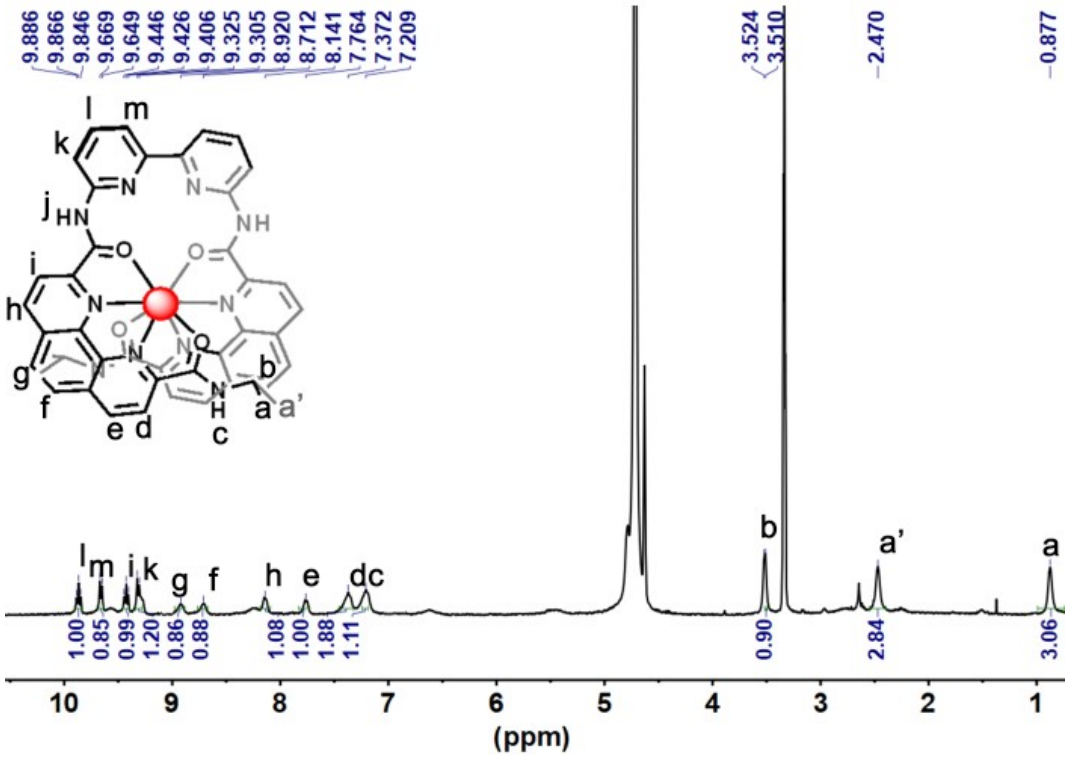

Figure S19. ^{1}H NMR spectrum of complex **EuL(OTf)$_3$** (400 MHz, CD_3CN/CD_3OD v/v = 4/1, 298 K).

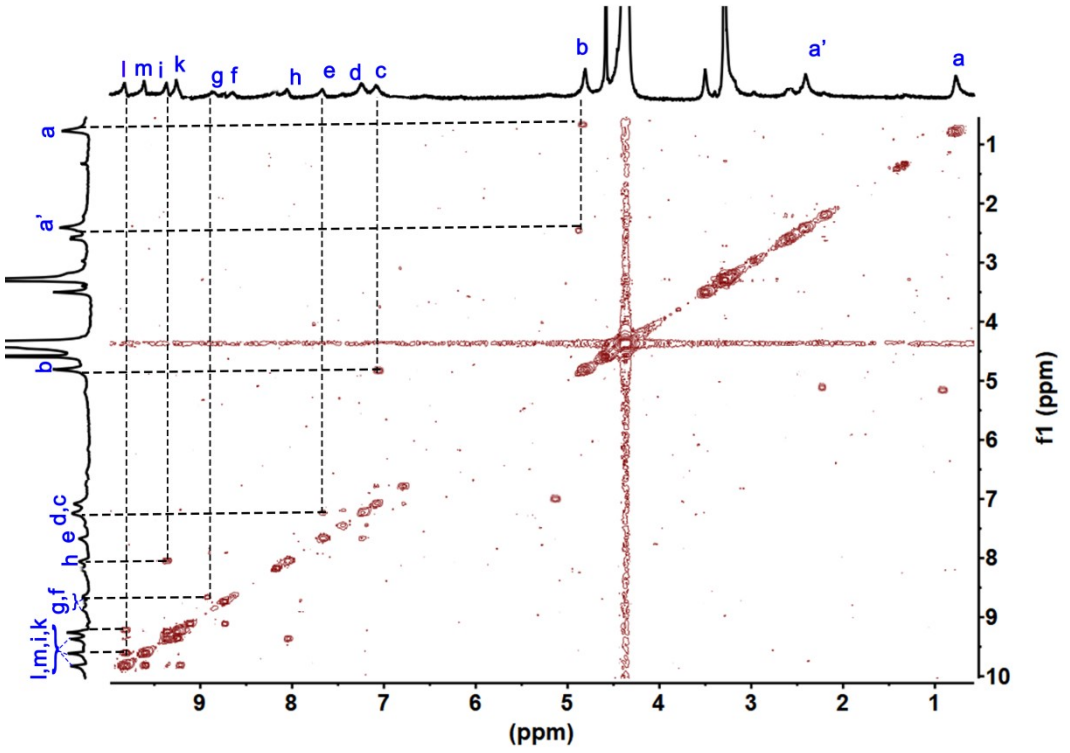

Figure S20. ^{1}H-^{1}H COSY NMR spectrum of complex **EuL(OTf)$_3$** (400 MHz, CD_3CN/CD_3OD v/v = 4/1, 298 K).

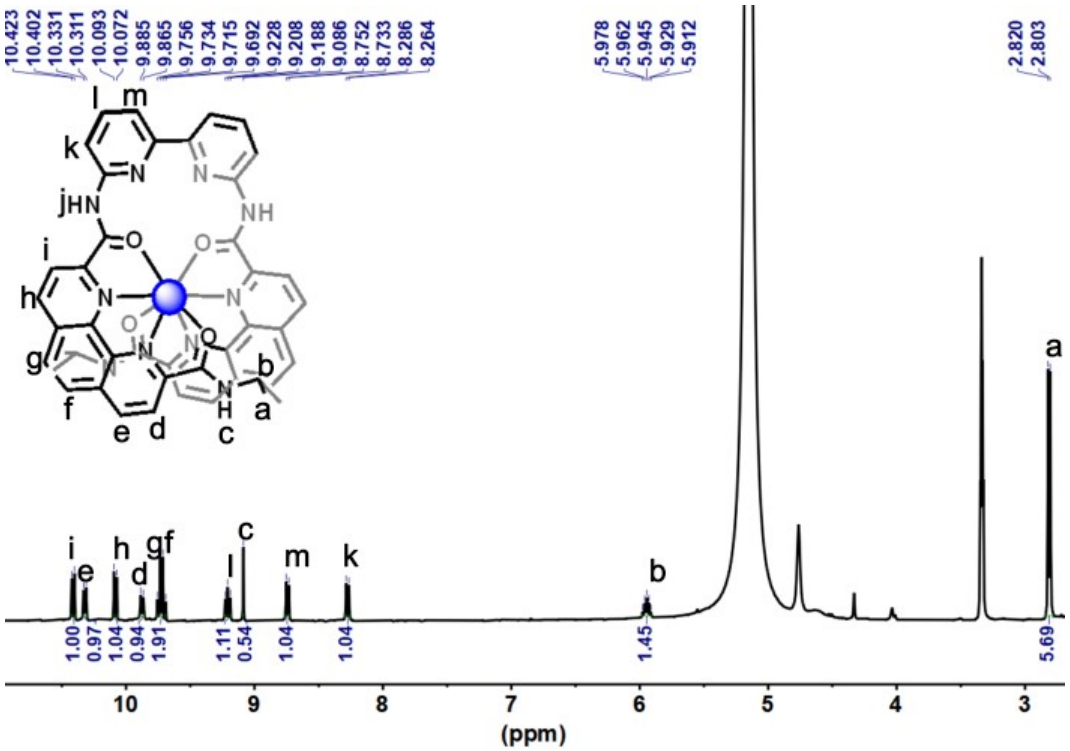

Figure S21. ^{1}H NMR spectrum of complex **LuL(OTf)$_3$** (400 MHz, CD_3CN/CD_3OD v/v = 4/1, 298 K).

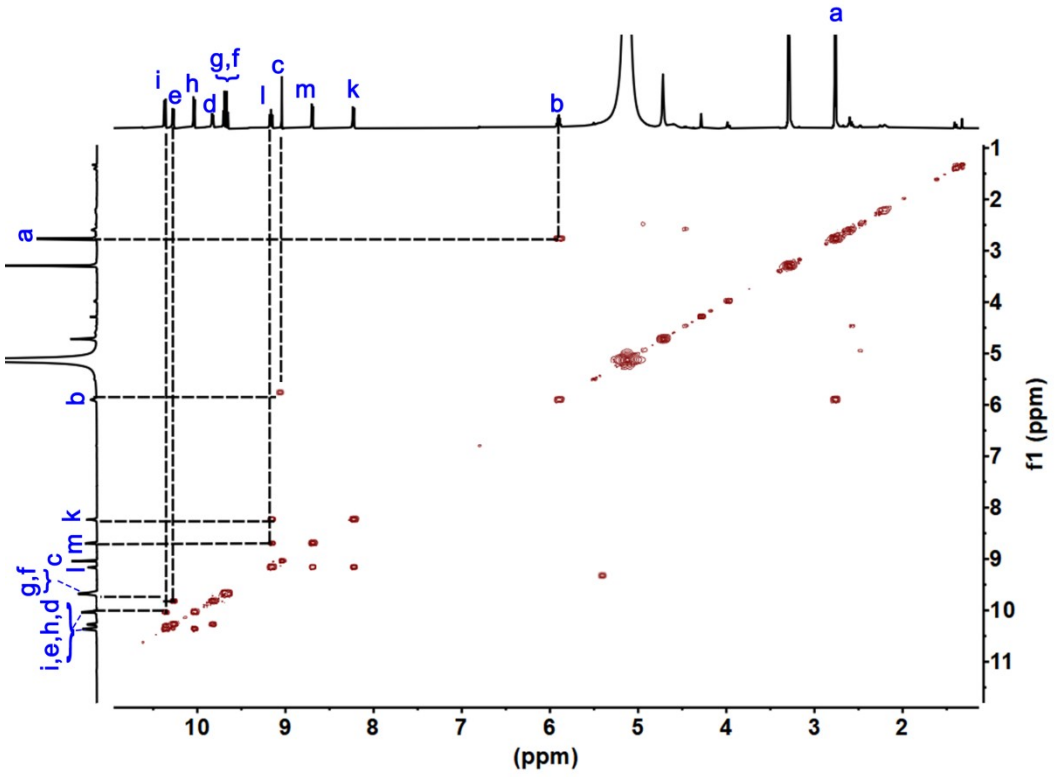

Figure S22. ^{1}H-^{1}H COSY NMR spectrum of complex **LuL(OTf)$_3$** (400 MHz, CD_3CN/CD_3OD v/v = 4/1, 298 K).

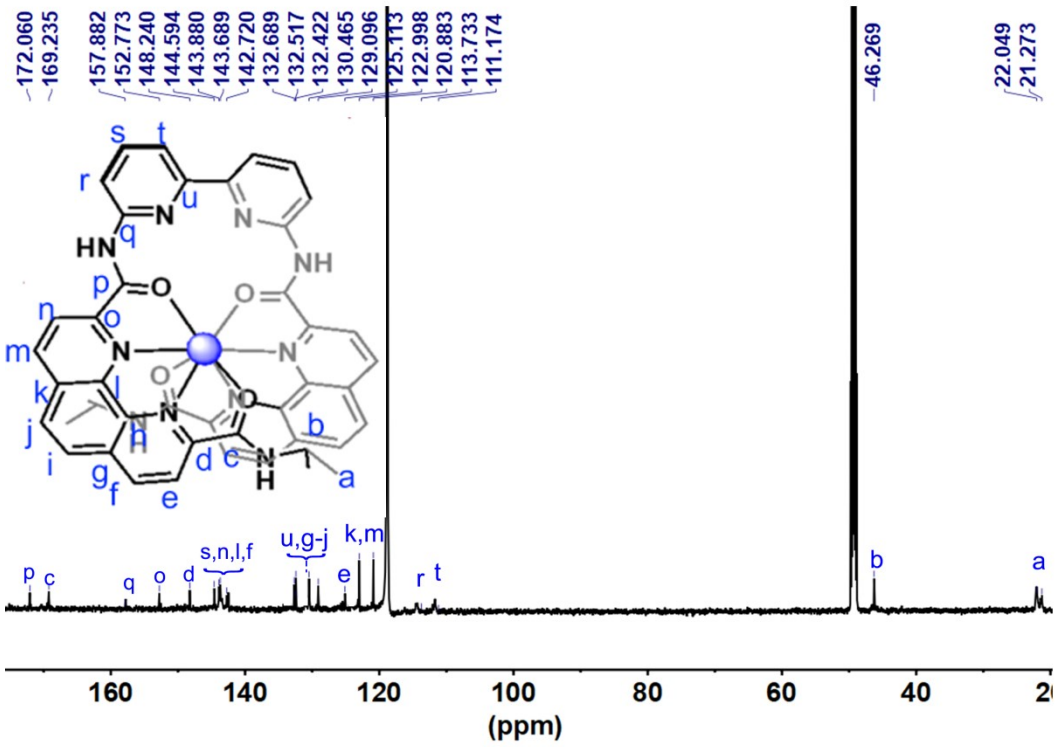

Figure S23. ^{13}C NMR spectrum of complex **LuL(OTf)$_3$** (151 MHz, CD_3CN/CD_3OD v/v = 4/1, 298 K).

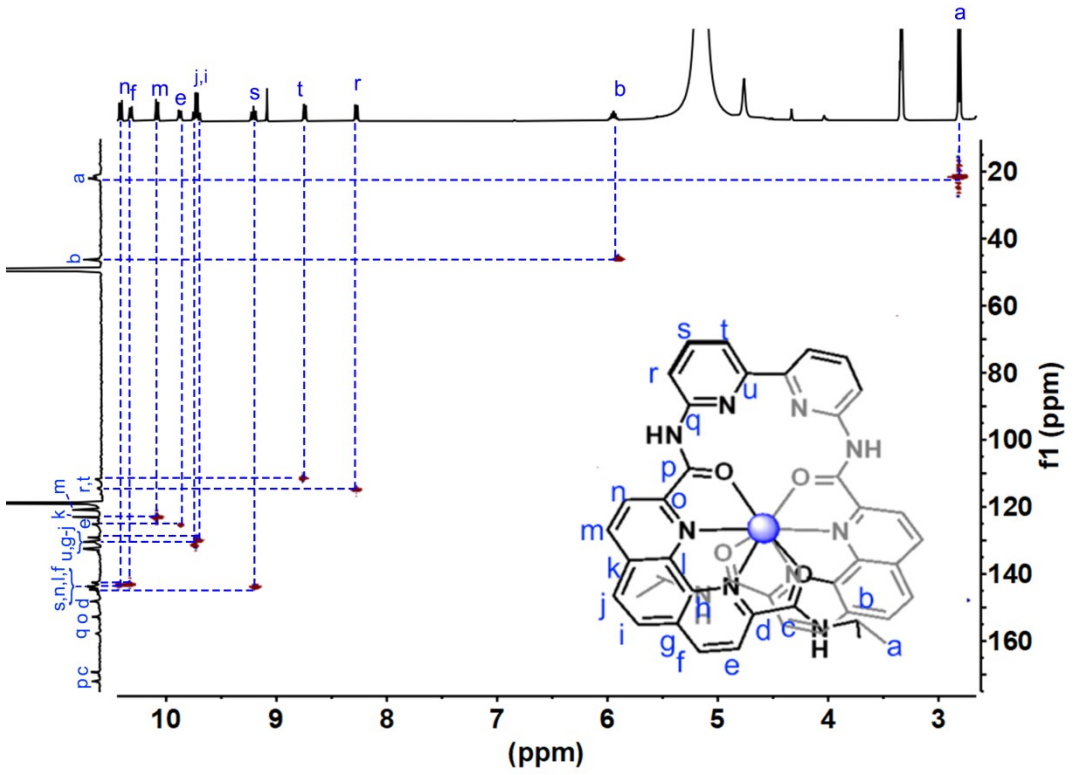

Figure S24. ^{1}H-{^{13}C} HSQC spectrum of **LuL(OTf)$_3$** (600 MHz, CD_3CN/CD_3OD v/v = 4/1, 298 K).

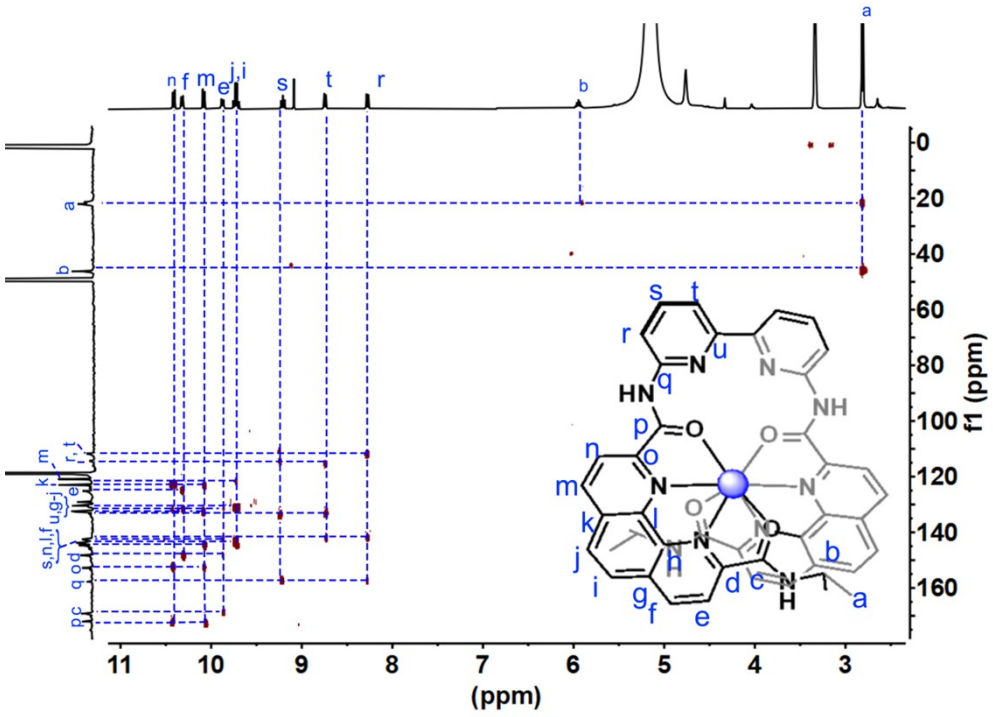

Figure S25. ^{1}H-{^{13}C} HMBC spectrum of **LuL(OTf)$_3$** (CD_3CN/CD_3OD v/v = 4/1, 298 K).

DOSY spectra were applied to estimate the dynamic radius according to the Stokes-Einstein equation[S2] :

$$D = \frac{TK_B}{6\pi\eta r} \quad (1)$$

Where: D is diffusion coefficient obtained from DOSY spectrum, K_B is Boltzmann constant, T is temperature, viscosity Z was tested to be 2.2 mPa s and r is the estimated dynamic radius.

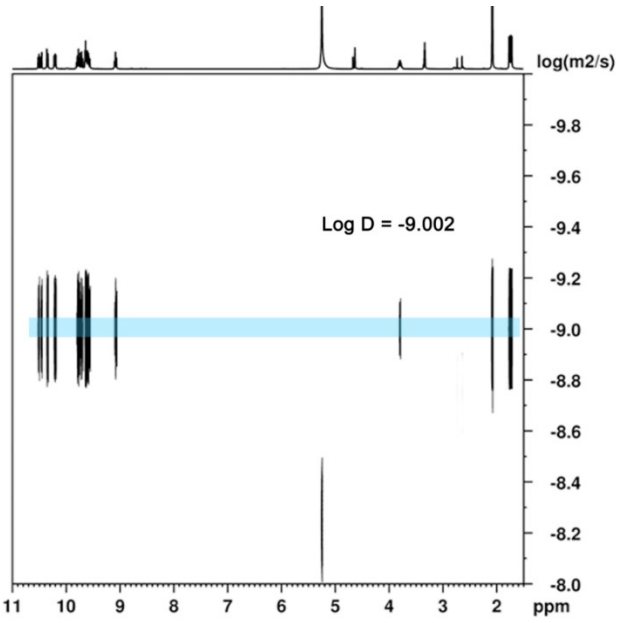

Figure S26. ^{1}H-^{1}H DOSY spectrum of **LaL(OTf)$_3$** (CD_3CN/CD_3OD v/v = 4/1, 400 MHz, 298 K).

$D = 9.54 \times 10^{-10}$ m^2s^{-1}

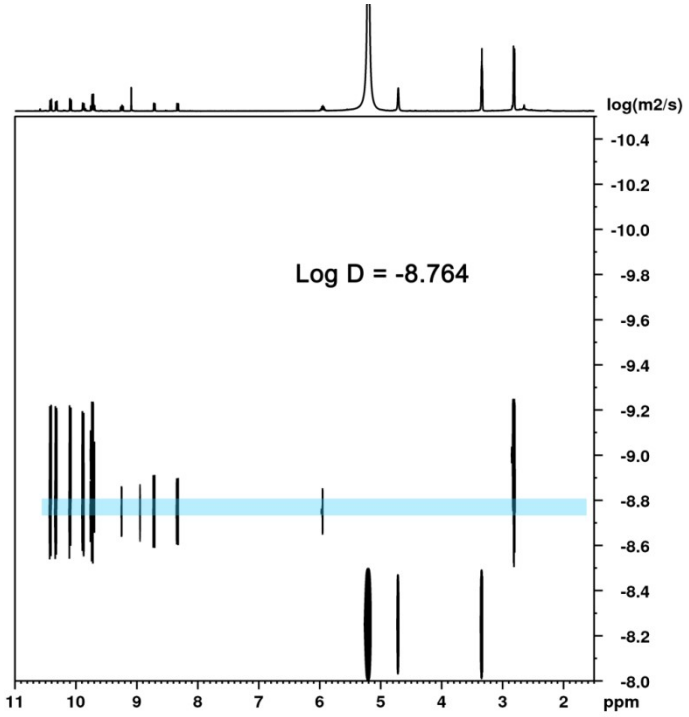

Figure S27. ^{1}H-^{1}H DOSY spectrum of **LuL(OTf)$_3$** (CD_3CN/CD_3OD v/v = 4/1, 400 MHz, 298 K).

$D = 1.737 \times 10^{-9}\ m^2s^{-1}$.

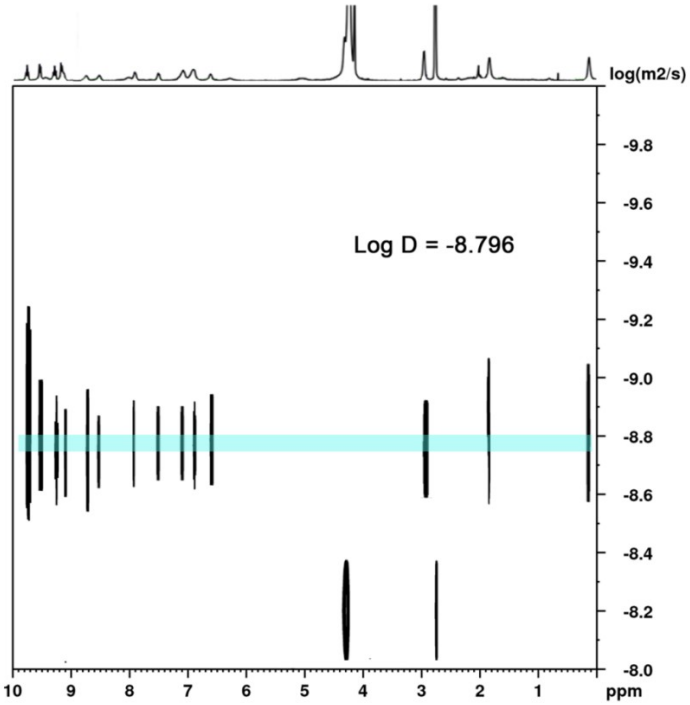

Figure S28. ^{1}H-^{1}H DOSY spectrum of **EuL(OTf)$_3$** (CD_3CN/CD_3OD v/v = 4/1, 400 MHz, 298 K).

$D = 1.403 \times 10^{-9}\ m^2s^{-1}$.

4. Photophysical properties

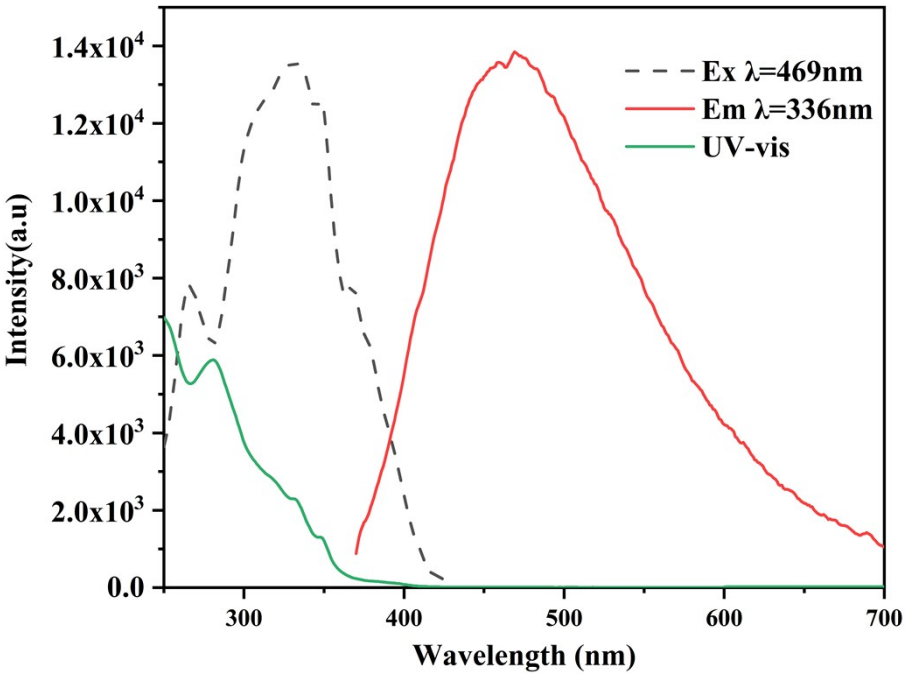

Figure S29. UV-vis, excitation and emission spectra of **L** in $CHCl_3$ (298 K, $c = 1.5\times10^{-5}$ M).

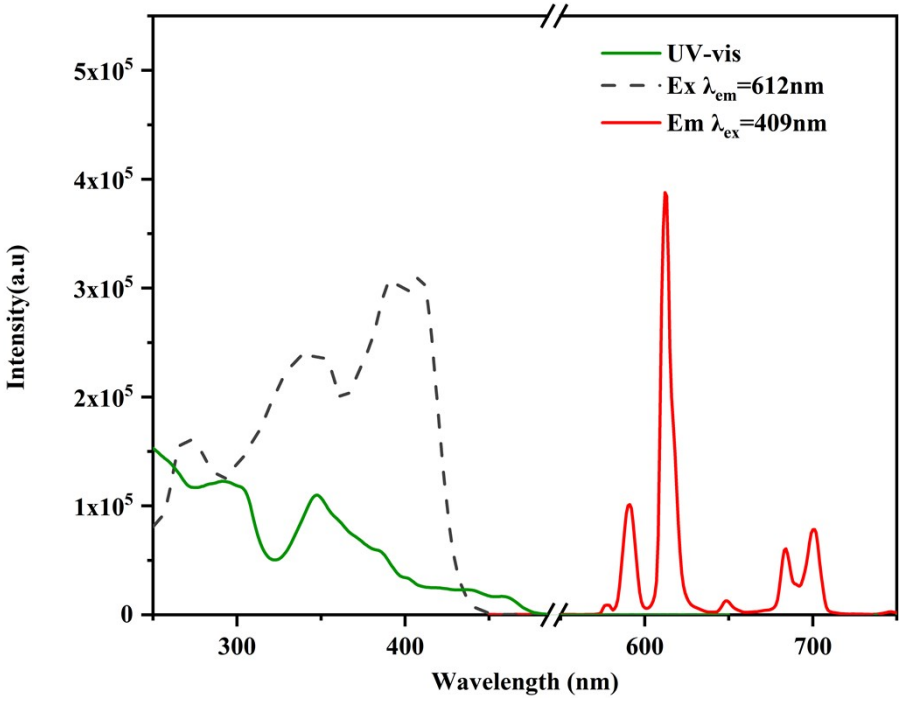

Figure S30. UV-vis, excitation and emission spectra of complex **EuL(OTf)$_3$** in CH_3CN (298 K, $c = 1\times10^{-5}$ M).

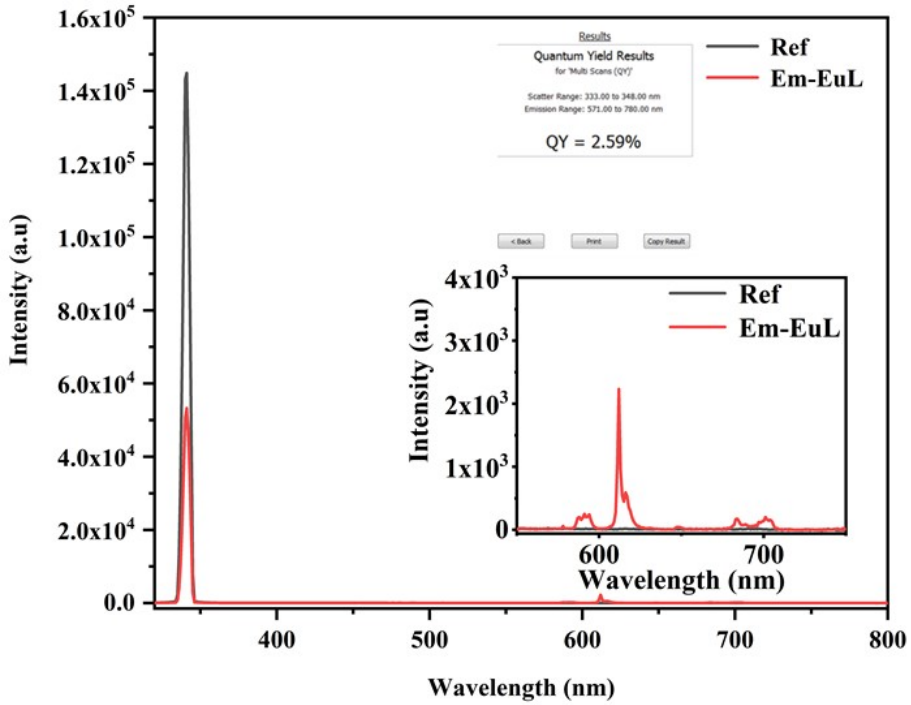

Figure S31. Luminescent quantum yield of complex **EuL(OTf)$_3$** in CH_3CN (298 K, c = 1×10^{-5} M, λ_{ex} = 409 nm, slit: 5.0-0.58）

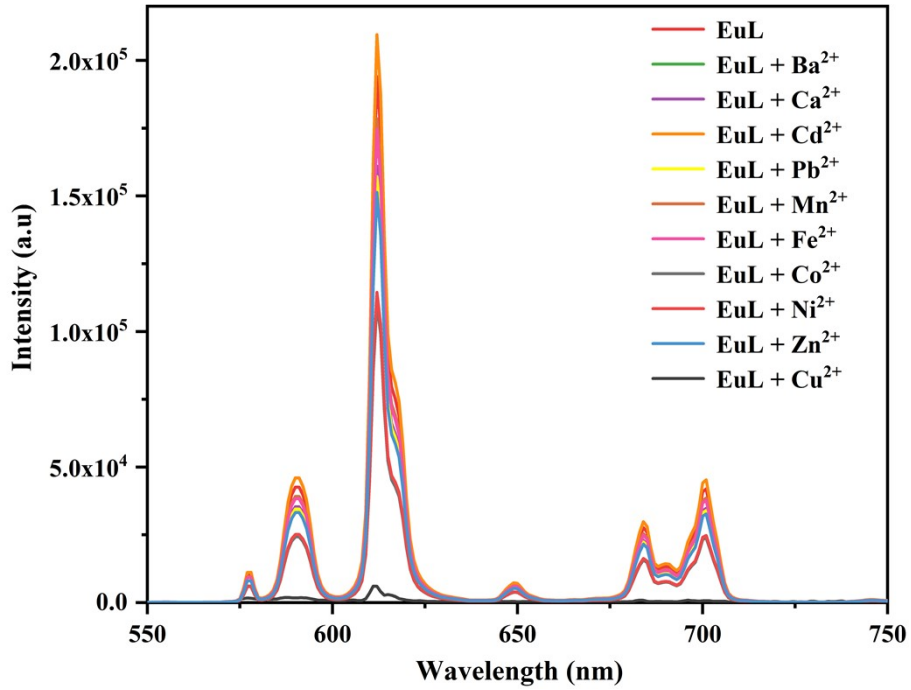

Figure S32. Luminescent titration spectra of **EuL(OTf)$_3$** in CH_3CN (298 K, c = 1.2×10^{-5} M, λ_{ex} = 409 nm) upon addition of 2 equiv of various metal cation (ClO_4^- salt).

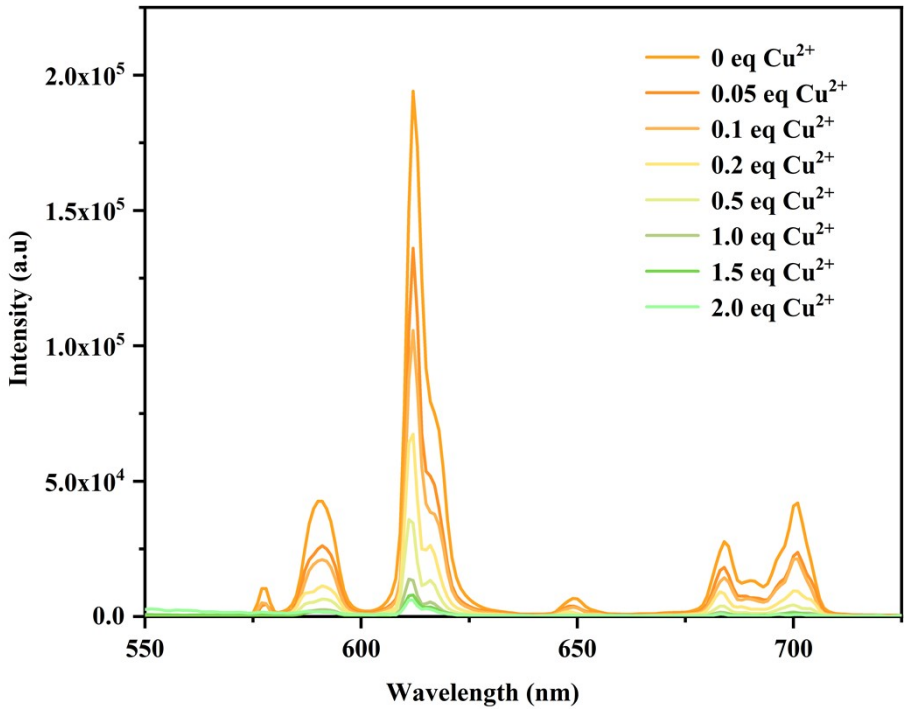

Figure S33. Luminescent titration spectra of **EuL(OTf)$_3$** in CH_3CN (298 K, c = 1.2×10^{-5} M, λ_{ex} = 409 nm) upon addition of different equiv of Cu^{2+} (ClO_4^- salt).

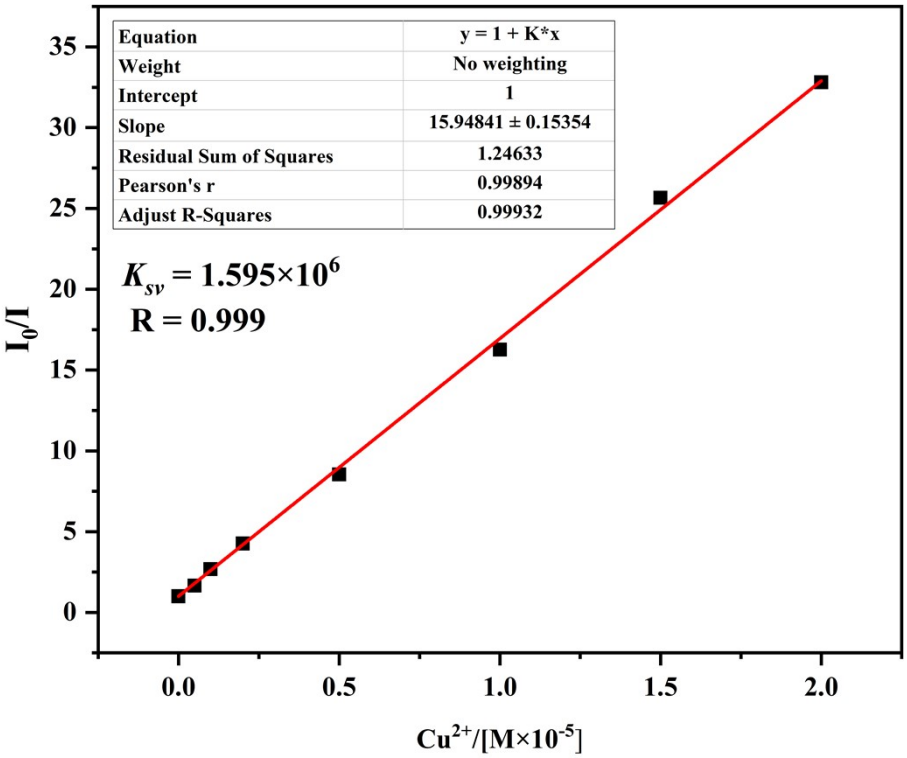

Figure S34. Stern-Volmer plot ($I_0/I = K_{SV}[Cu^{2+}] + 1$) obtained from the titration results shown in **Figure S25**. (λ_{ex} = 409 nm, Intensities at λ_{em} = 612 nm)

5. UV-vis titration spectra and the determination of binding constant

The binding constant K_a were determined from the following Benesi-Hildebrand equation[S3]

$$\frac{1}{A - A_0} = \frac{a}{a - b}\left[\frac{1}{K[M]} + 1\right]$$

Where K = Binding constant;

A_0 = The observed absorption in the absence of metal cation;

A = The observed absorption with the metal cation added;

[M] = The concentration of the metal cation;

a and b are constants, the binding constant value K was evaluated graphically by plotting 1/ΔA against 1/[M].

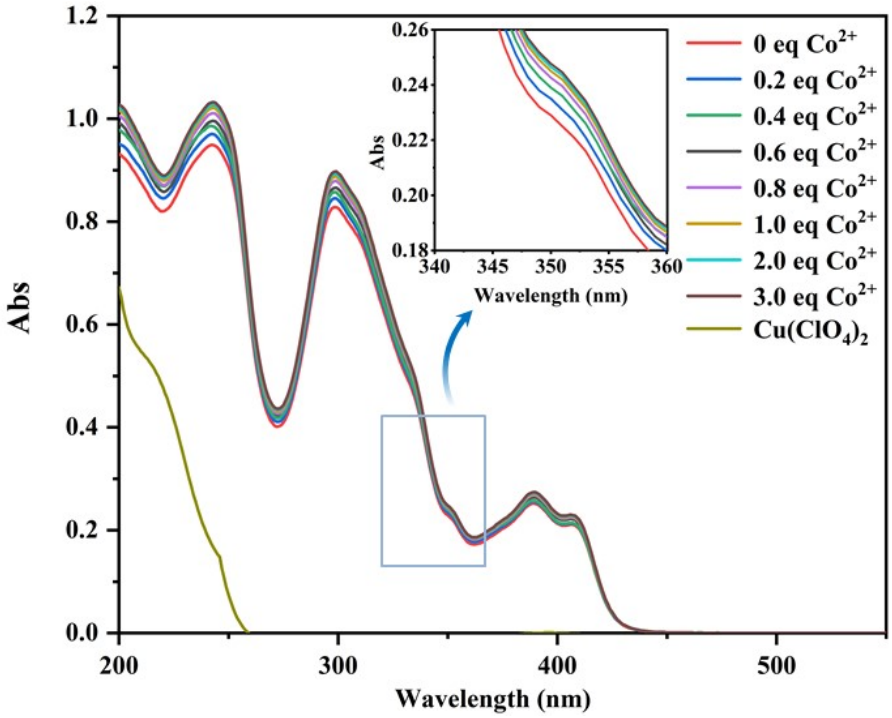

Figure S35. After adding different equivalents of $Co(ClO_4)_2$, the UV-vis titration spectra of **LaL(OTf)$_3$** in CH_3CN (c = 1.0×10^{-5} M) (Inset shows peak intensity change at 351 nm).

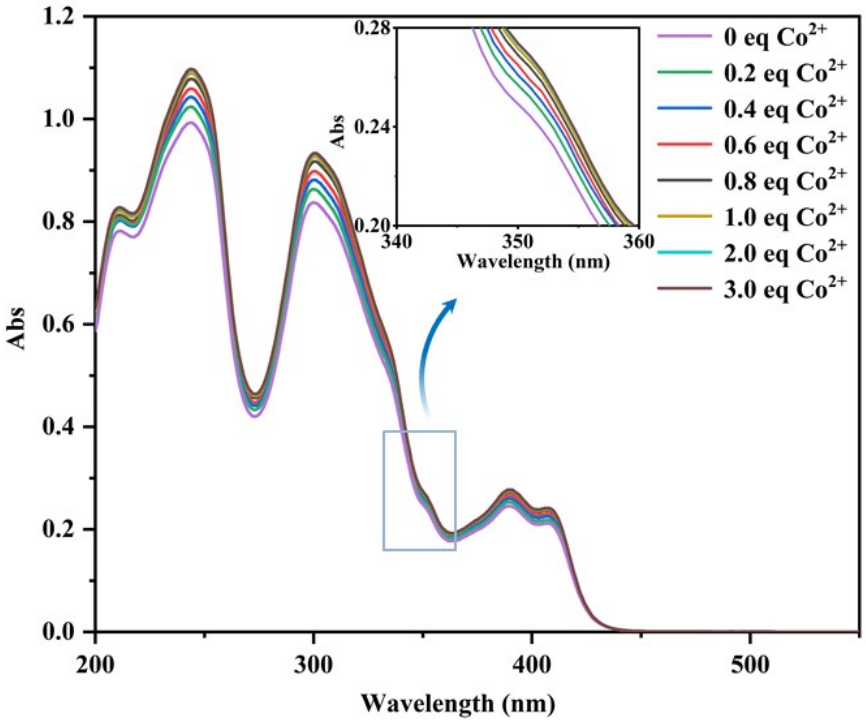

Figure S36. After adding different equivalents of $Co(ClO_4)_2$, the UV-vis titration spectra of **EuL(OTf)$_3$** in CH_3CN (c = 1.0×10^{-5} M) (Inset shows peak intensity change at 351 nm).

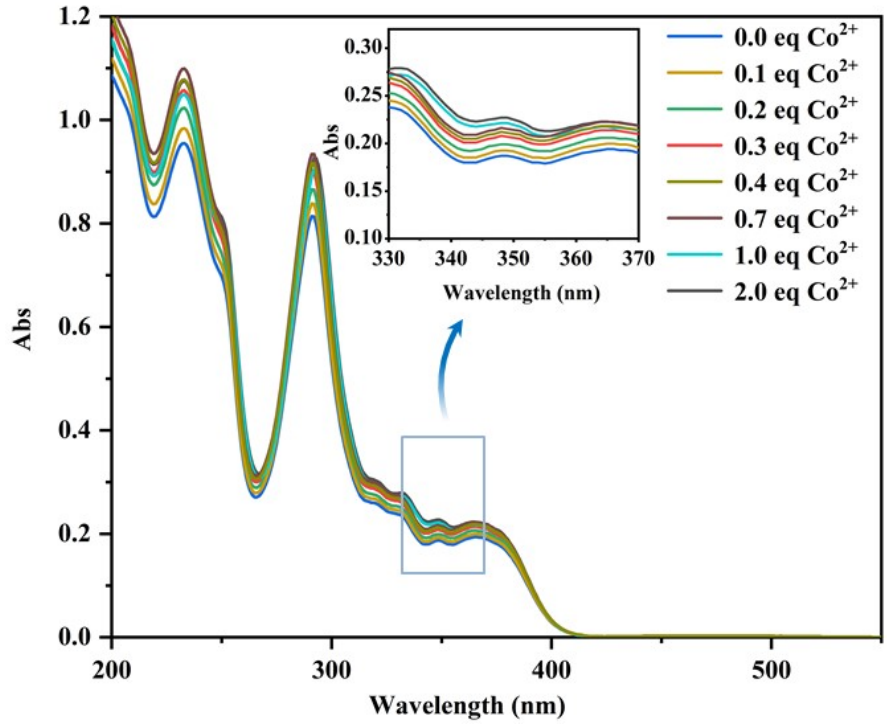

Figure S37. After adding different equivalents of $Co(ClO_4)_2$, the UV-vis titration spectra of **LuL(OTf)$_3$** in CH_3CN (c = 1.0×10^{-5} M) (Inset shows peak intensity change at 351 nm).

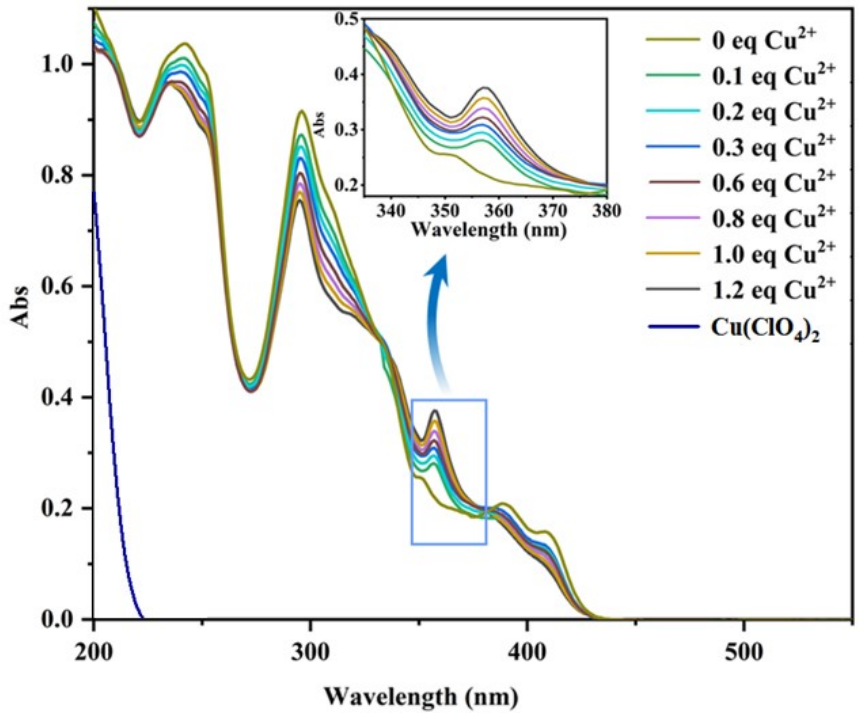

Figure S38. After adding different equivalents of $Cu(ClO_4)_2$, the UV-vis titration spectra of **LaL(OTf)$_3$** in CH_3CN ($c = 1.0\times10^{-5}$ M) (Inset shows peak intensity change at 358 nm).

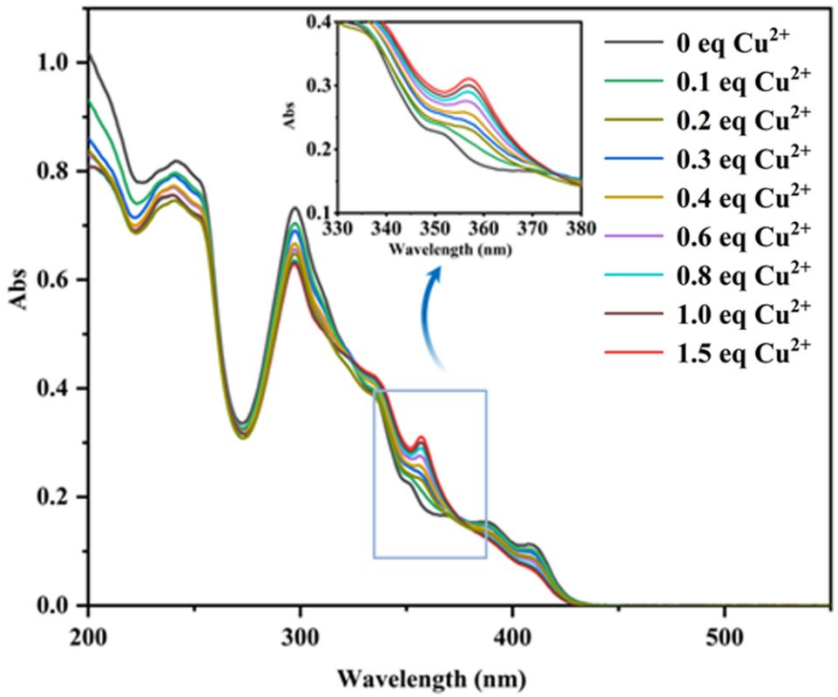

Figure S39. After adding different equivalents of $Cu(ClO_4)_2$, the UV-vis titration spectra of **EuL(OTf)$_3$** in CH_3CN ($c = 1.0\times10^{-5}$ M) (Inset shows peak intensity change at 358 nm).

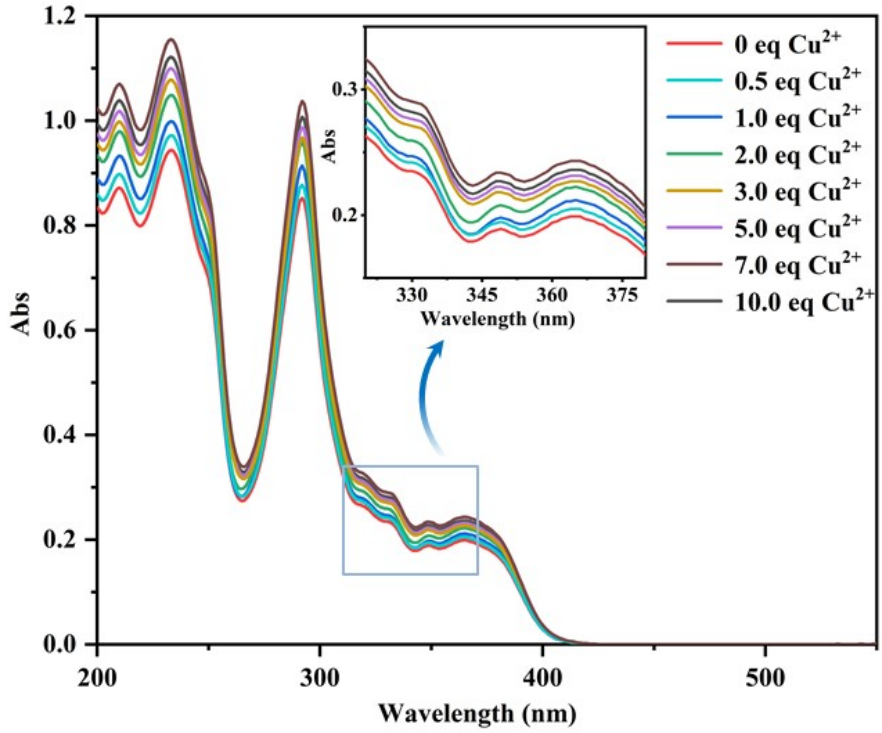

Figure S40. After adding different equivalents of $Cu(ClO_4)_2$, the UV-vis titration spectra of **LuL(OTf)$_3$** in CH_3CN ($c = 1.0\times10^{-5}$ M) (Inset shows peak intensity change at 358 nm).

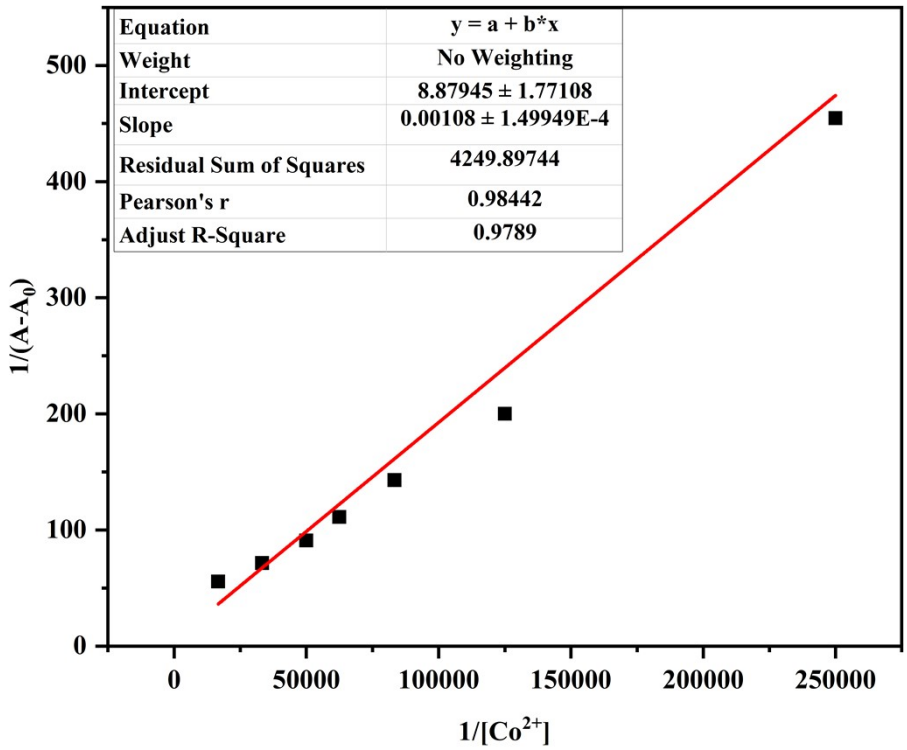

Figure S41. Benesi-Hilderbrand plot of **LaL(OTf)$_3$** and Co^{2+} based on the change in the intensity of the 351 nm peak in **Figure S35.**

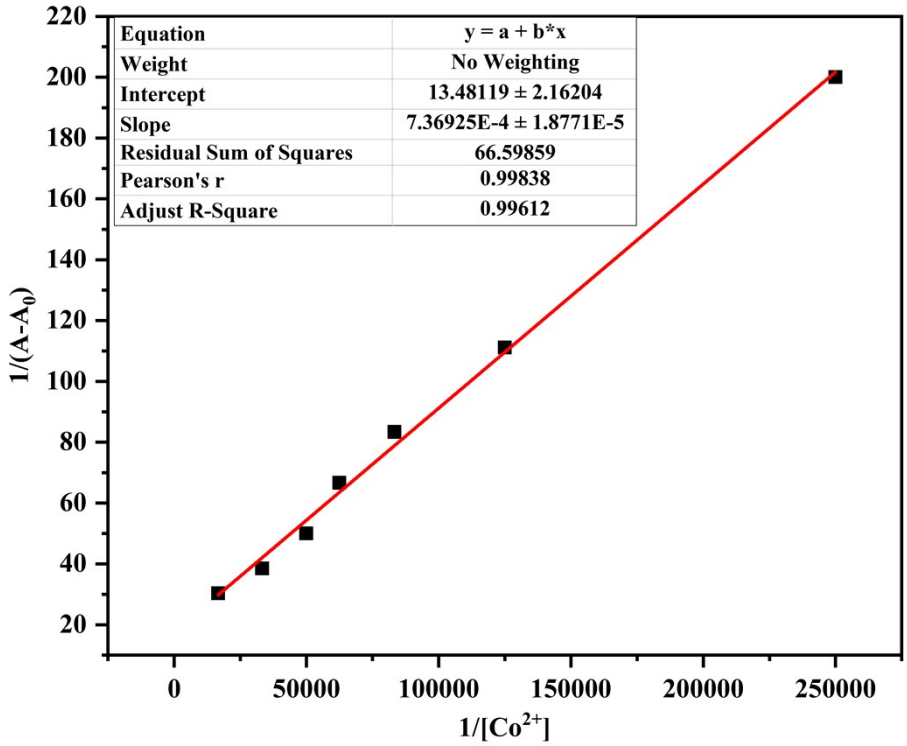

Figure S42. Benesi-Hilderbrand plot of **EuL(OTf)$_3$** and Co^{2+} based on the change in the intensity of the 351 nm peak in **Figure S36.**

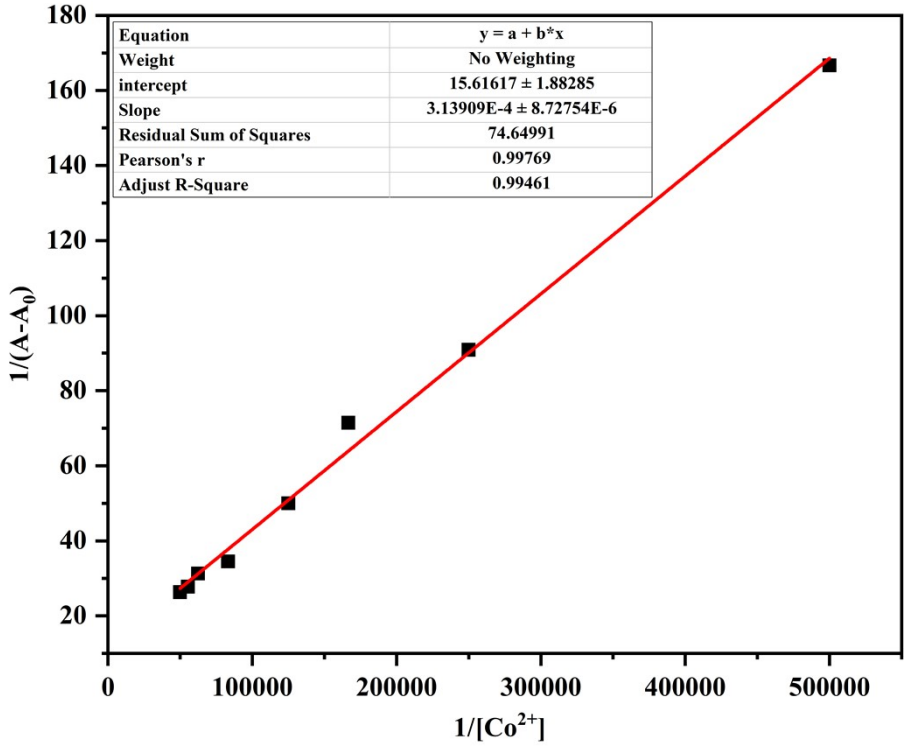

Figure S43. Benesi-Hilderbrand plot of **LuL(OTf)$_3$** and Co^{2+} based on the change in the intensity of the 351 nm peak in **Figure S37**.

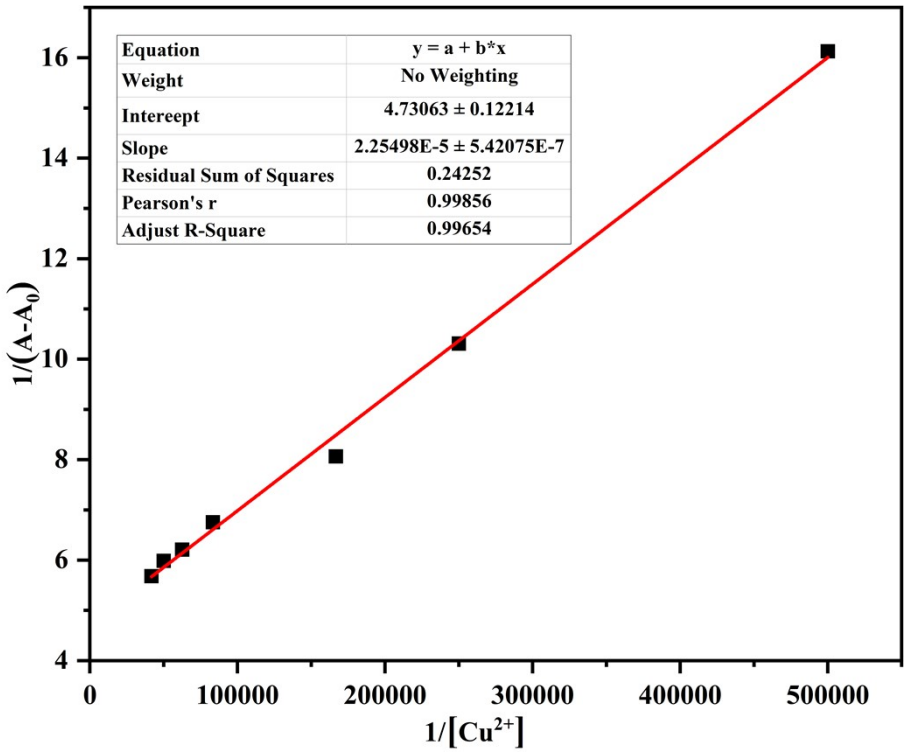

Figure S44. Benesi-Hilderbrand plot of **LaL(OTf)$_3$** and Cu^{2+} based on the change in the intensity of the 358 nm peak in **Figure S38**.

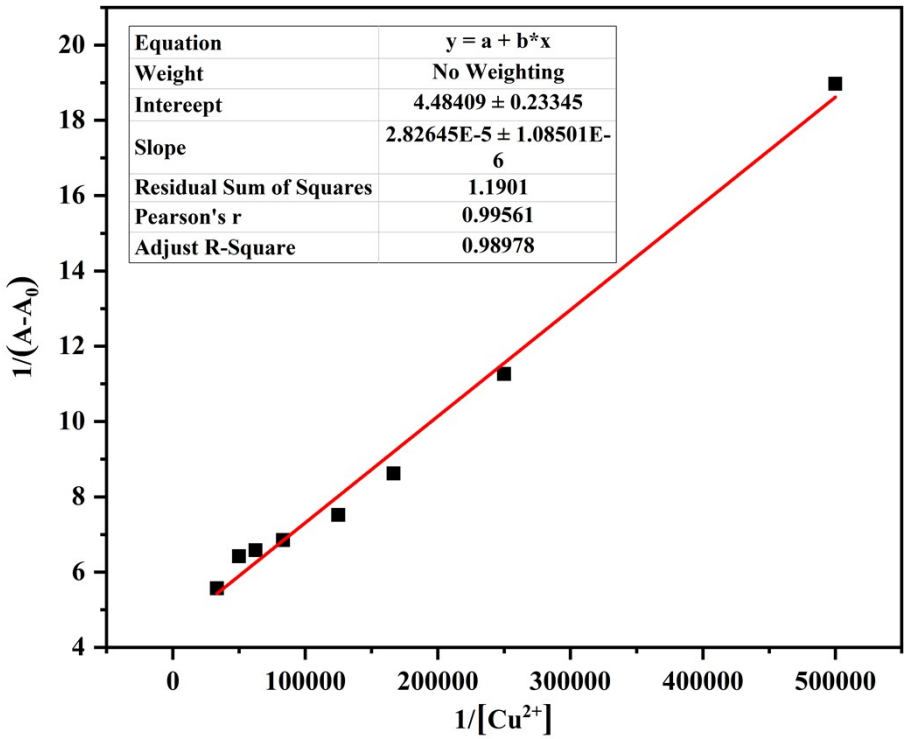

Figure S45. Benesi-Hilderbrand plot of **EuL(OTf)$_3$** and Cu^{2+} based on the change in the intensity of the 358 nm peak in **Figure S39**.

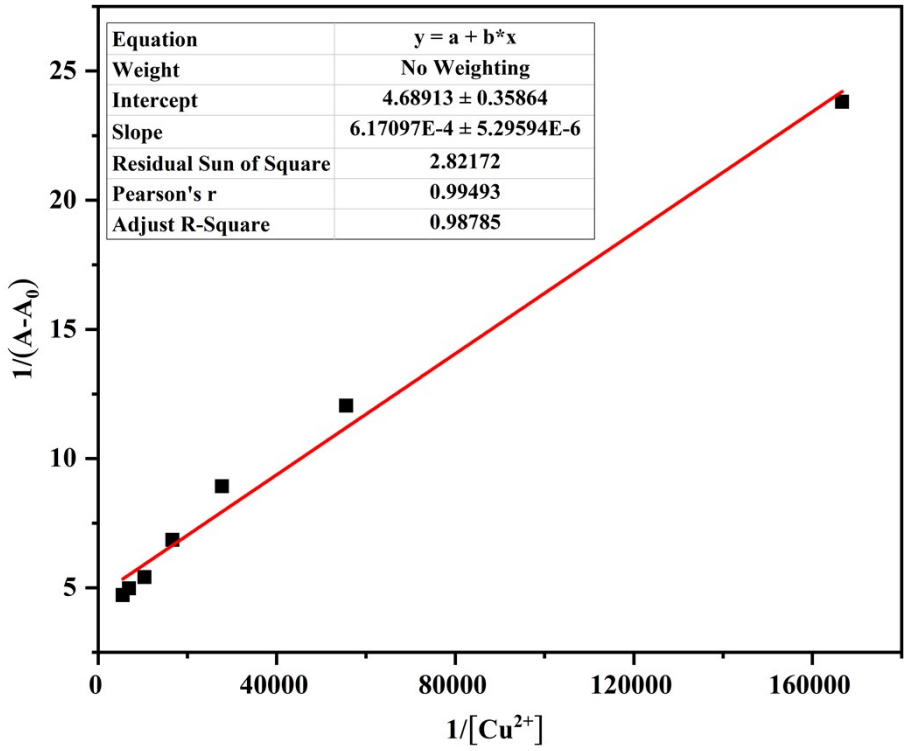

Figure S46. Benesi-Hilderbrand plot of **LuL(OTf)$_3$** and Cu^{2+} based on the change in the intensity of the 358 nm peak in **Figure S40**.

Table S1. Summary of bonding Constants K_a

	$LaL(OTf)_3$	$EuL(OTf)_3$	$LuL(OTf)_3$
$Co(ClO_4)_2$	$8.22 \pm 0.494 \times 10^3\ M^{-1}$	$1.29 \pm 0.127 \times 10^4\ M^{-1}$	$4.97 \pm 0.462 \times 10^4\ M^{-1}$
$Cu(ClO_4)_2$	$2.10 \pm 0.003 \times 10^5\ M^{-1}$	$1.58 \pm 0.007 \times 10^5\ M^{-1}$	$7.59 \pm 0.514 \times 10^3\ M^{-1}$

6. ESI-TOF-MS spectra

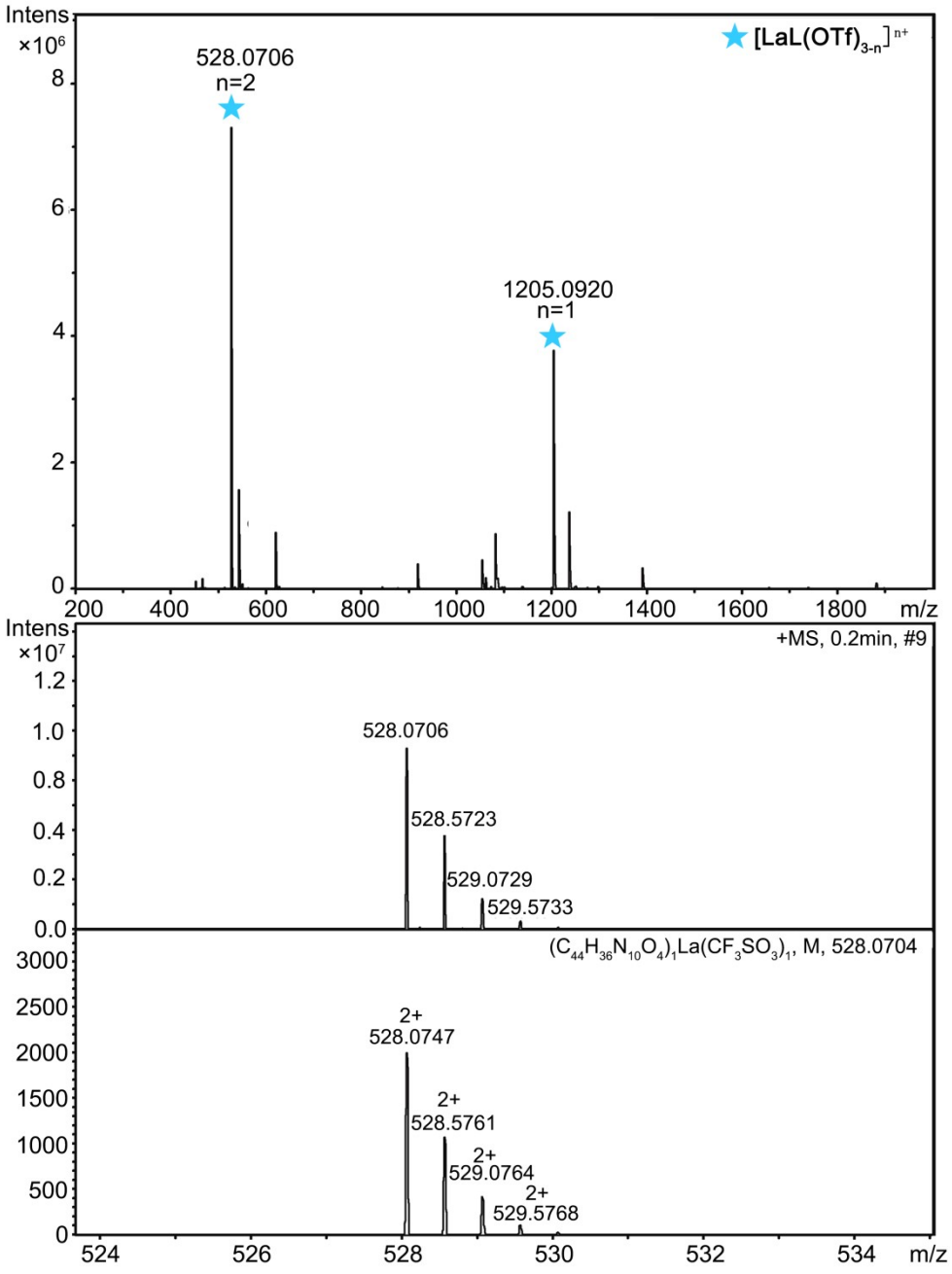

Figure S47. HR-ESI-TOF-MS of complex La**L**, the observed and calculated isotopic patterns of the peak 2+.

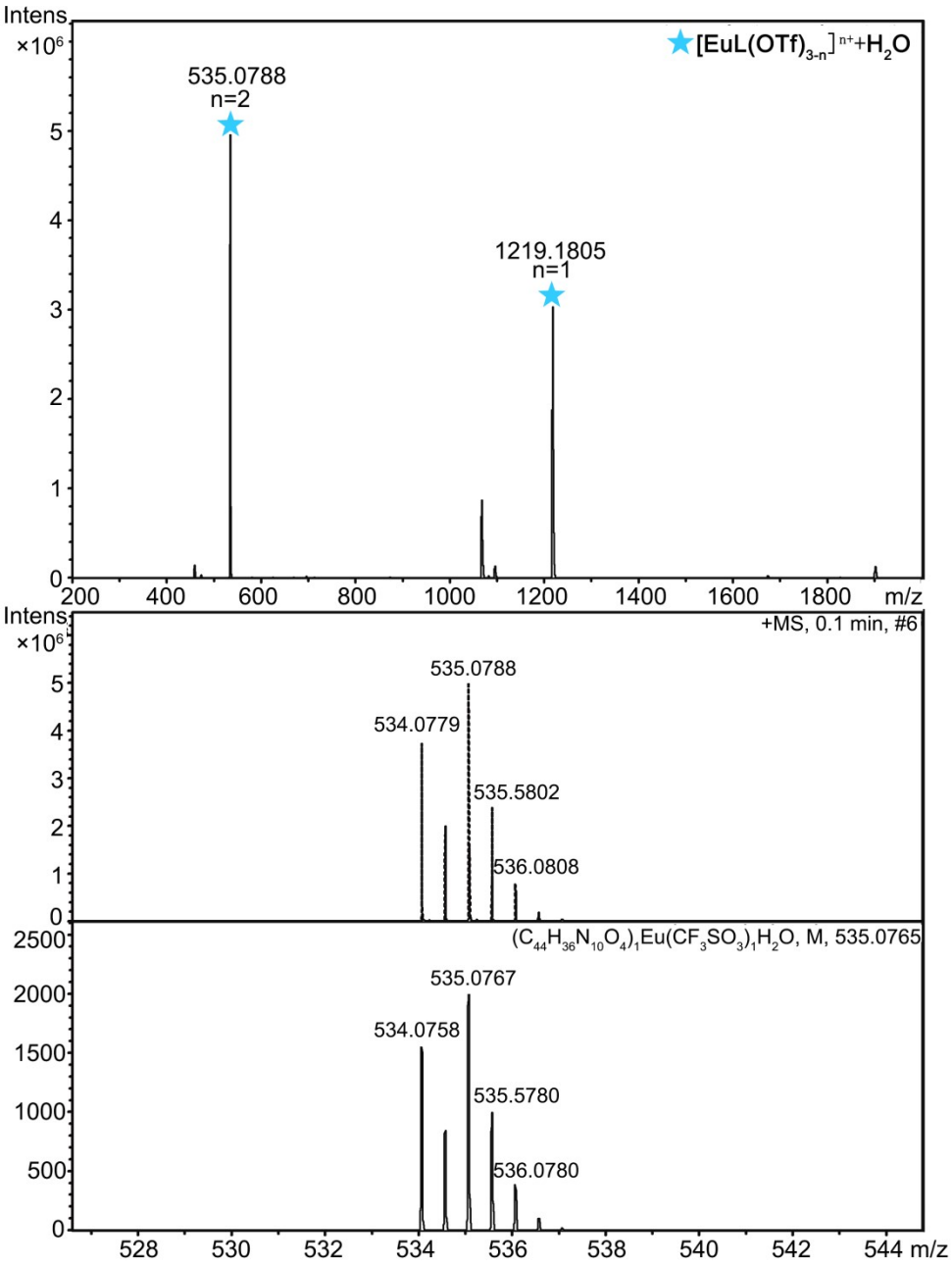

Figure S48. HR-ESI-TOF-MS of complex Eu**L**, the observed and calculated isotopic patterns of the peak 2+.

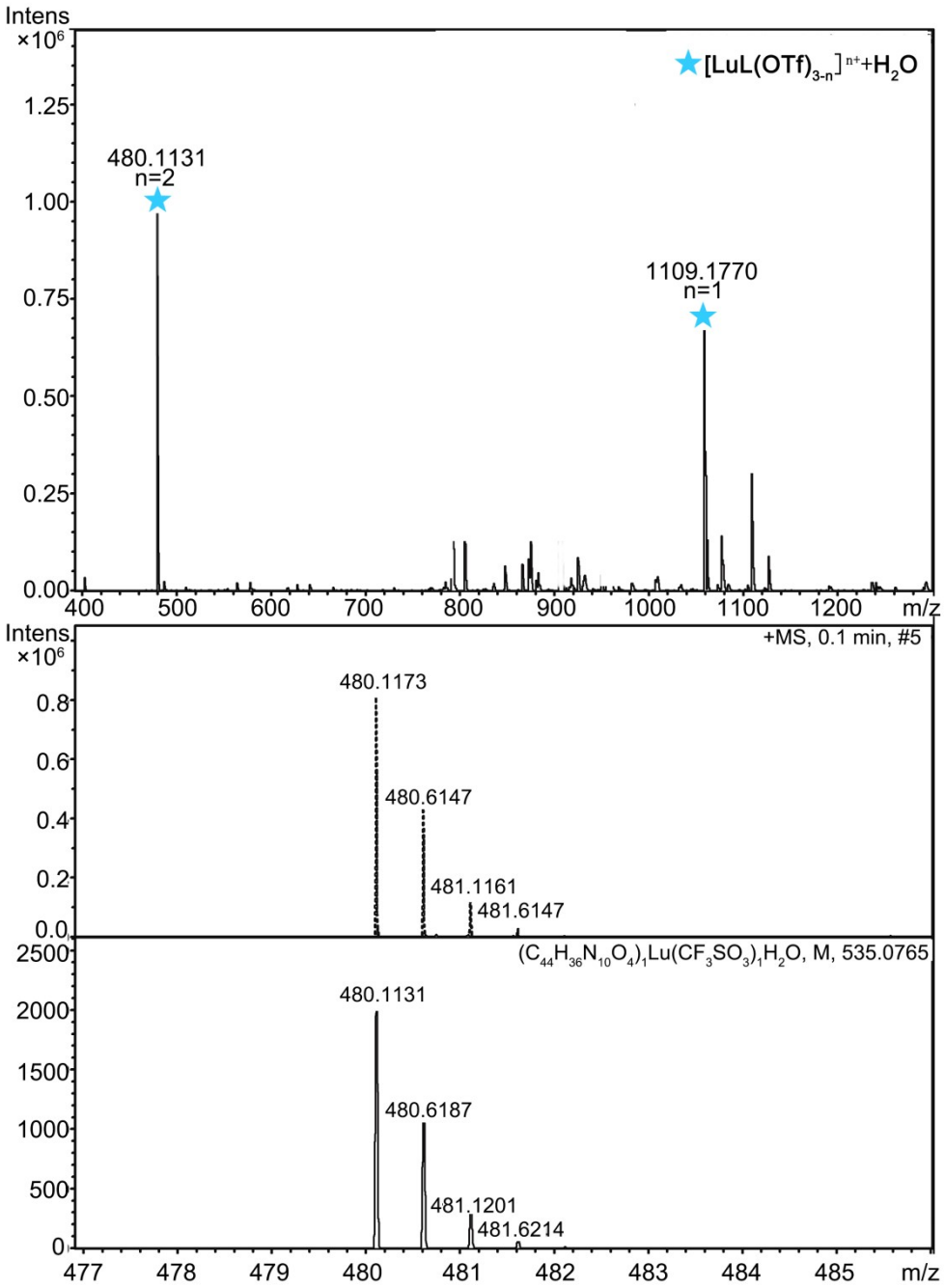

Figure S49. HR-ESI-TOF-MS of complex Lu**L**, the observed and calculated isotopic patterns of the peak 2+.

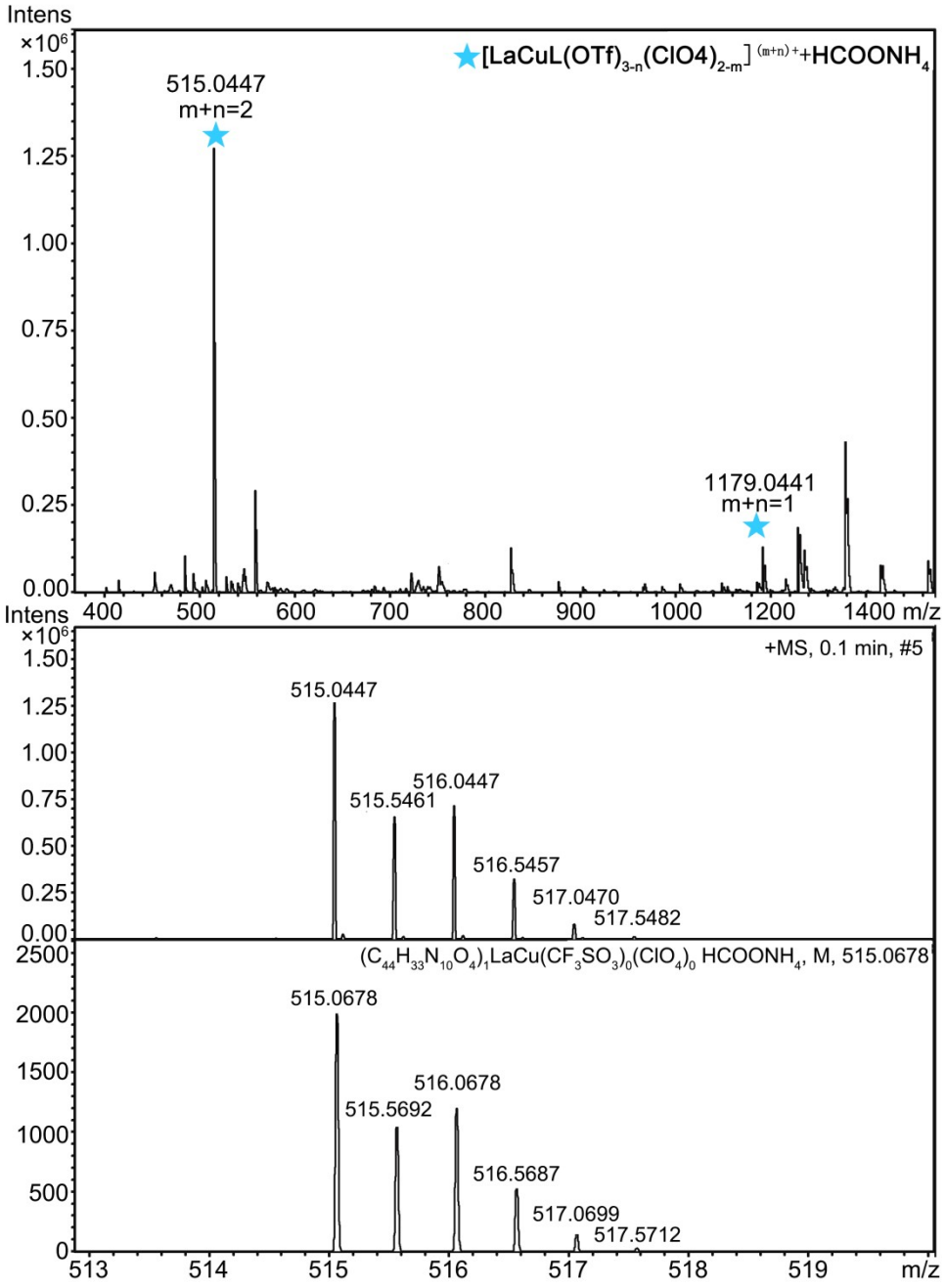

Figure S50. HR-ESI-TOF-MS of complex LaCu**L**, the observed and calculated isotopic patterns of the peak 2+.

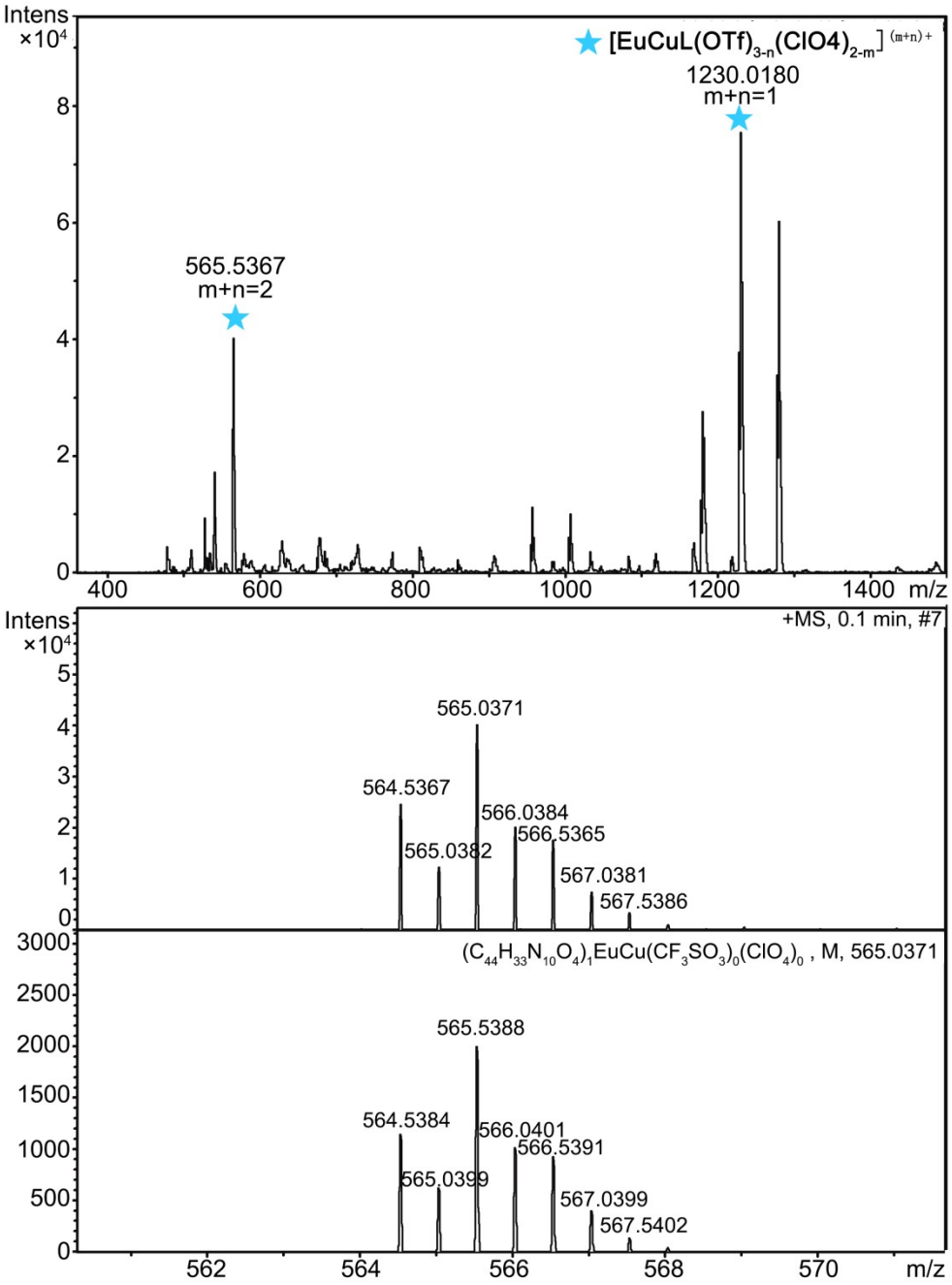

Figure S51. HR-ESI-TOF-MS of complex EuCu**L**, the observed and calculated isotopic patterns of the peak 2+.

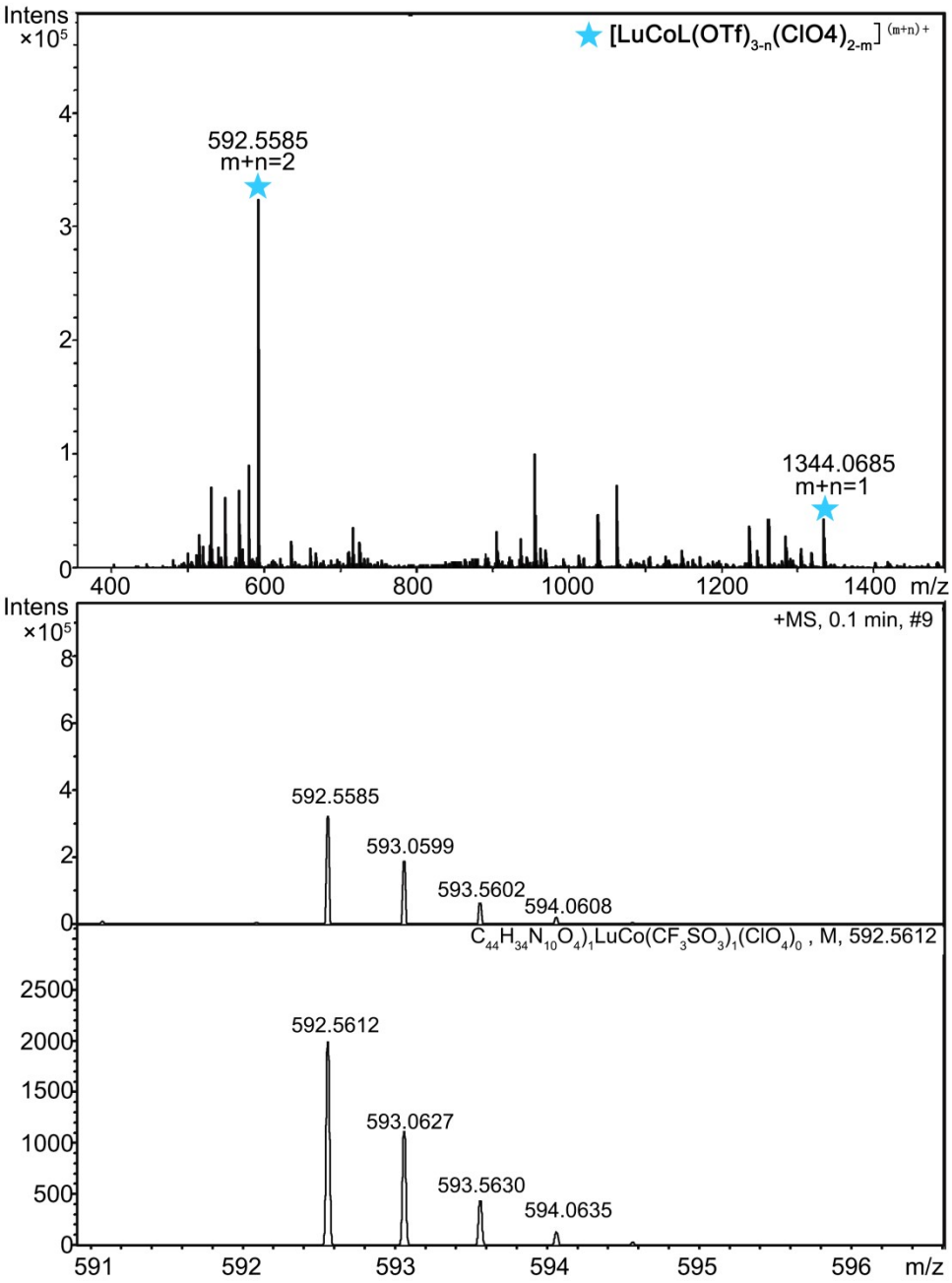

Figure S52. HR-ESI-TOF-MS of complex LuCo**L**, the observed and calculated isotopic patterns of the peak 2+.

7. Single crystal X-ray diffraction studies

Suitable crystals for La**L**, Eu**L**, LaCu**L** and EuCu**L** were obtained by slow diffision of poor solvent into solution of the corresponding complexes (MeCN/MeOH, v/v = 4/1) at room temperature for one to two weeks. The X-ray diffraction for Eu**L** was carried out on micro-focus metaljet diffractometer using Ga Kα radiation (λ = 1.3405 Å). Data reduction was performed with the CrysAlisPro package[S4]. The X-ray diffraction for other complexes were carried out on Bruker D8 VENTURE photon II diffractometer with Iμs 3.0 microfocus X-ray source using APEX III

program. And an analytical absorption correction was performed. Data reduction was performed with the saint and SADABS package[S5]. The structures were solved by direct methods and refined by full-matrix least-squares on F^2 with anisotropic displacement using the SHELX software package[S6]. The electron residuals in such cases were removed by the PLATON/SQUEEZE routine[S7]. Details on crystal data collection and refinement were summarized in Tables S2-5. CCDC: 2155931-2155934.

Table S2. Crystal data and structure refinement for La**L**.

Identification code	La**L**	
Empirical formula	$C_{49}H_{44}F_9LaN_{10}O_{15}S_3$ [+solvent]	
Formula weight	1419.03	
Temperature	170(2) K	
Wavelength	0.71073 Å	
Crystal system	Triclinic	
Space group	P-1	
Unit cell dimensions	a = 12.2691(12) Å	a= 80.485(4)°.
	b = 12.5181(12) Å	b= 83.793(4)°.
	c = 21.061(2) Å	g = 87.269(4)°.
Volume	3169.9(5) $Å^3$	
Z	2	
Density (calculated)	1.487 Mg/m^3	
Absorption coefficient	0.867 mm^{-1}	
F(000)	1428	
Crystal size	0.1 x 0.1 x 0.05 mm^3	
Theta range for data collection	2.680 to 27.531°.	
Index ranges	-15<=h<=15, -16<=k<=16, -27<=l<=24	
Reflections collected	50582	
Independent reflections	14497 [R(int) = 0.0460]	
Completeness to theta = 25.242°	99.7 %	
Absorption correction	None	
Refinement method	Full-matrix least-squares on F^2	
Data / restraints / parameters	14497 / 816 / 789	
Goodness-of-fit on F^2	1.044	
Final R indices [I>2sigma(I)]	R1 = 0.0434, wR2 = 0.1173	
R indices (all data)	R1 = 0.0513, wR2 = 0.1240	
Extinction coefficient	n/a	
Largest diff. peak and hole	1.040 and -0.775 $e.Å^{-3}$	

Table S3. Crystal data and structure refinement for Eu**L**.

Identification code	Eu**L**	
Empirical formula	$C_{47}H_{38}EuF_9N_{10}O_{15}S_3$	
Formula weight	1402.01	
Temperature	293(2) K	
Wavelength	1.34139 Å	
Crystal system	Monoclinic	
Space group	C2/c	
Unit cell dimensions	a = 13.5398(2) Å	a= 90°.
	b = 23.7684(4) Å	b= 97.4176(17)°.
	c = 19.7203(5) Å	g = 90°.
Volume	6293.2(2) $Å^3$	
Z	4	
Density (calculated)	1.480 Mg/m^3	
Absorption coefficient	6.487 mm^{-1}	
F(000)	2808	
Crystal size	0.02 x 0.02 x 0.01 mm^3	
Theta range for data collection	3.235 to 48.749°.	
Index ranges	-13<=h<=15, -26<=k<=26, -22<=l<=21	
Reflections collected	24647	
Independent reflections	4637 [R(int) = 0.0448]	
Completeness to theta = 48.749°	99.7 %	
Absorption correction	Semi-empirical from equivalents	
Max. and min. transmission	1.00000 and 0.74285	
Refinement method	Full-matrix least-squares on F^2	
Data / restraints / parameters	4637 / 441 / 391	
Goodness-of-fit on F^2	1.041	
Final R indices [I>2sigma(I)]	R1 = 0.0694, wR2 = 0.2077	
R indices (all data)	R1 = 0.0778, wR2 = 0.2179	
Extinction coefficient	n/a	
Largest diff. peak and hole	1.709 and -0.601 $e.Å^{-3}$	

Table S4. Crystal data and structure refinement for LaCu**L**.

Identification code	LaCu**L**	
Empirical formula	$C_{45}H_{38}Cl_2CuF_3LaN_{10}O_{16}S$ [+ solvent]	
Formula weight	1337.28	
Temperature	200(2) K	
Wavelength	0.71073 Å	
Crystal system	Triclinic	
Space group	P-1	
Unit cell dimensions	a = 17.9309(11) Å	a= 87.266(2)°.
	b = 18.7163(14) Å	b= 63.594(2)°.
	c = 19.5429(14) Å	g = 86.071(2)°.
Volume	5859.4(7) $Å^3$	
Z	4	
Density (calculated)	1.516 Mg/m^3	
Absorption coefficient	1.289 mm^{-1}	
F(000)	2676	
Crystal size	0.2 x 0.2 x 0.1 mm^3	
Theta range for data collection	2.277 to 27.571°.	
Index ranges	-23<=h<=23, -24<=k<=24, -25<=l<=25	
Reflections collected	143890	
Independent reflections	27044 [R(int) = 0.0997]	
Completeness to theta = 25.242°	99.9 %	
Absorption correction	None	
Refinement method	Full-matrix least-squares on F^2	
Data / restraints / parameters	27044 / 1944 / 1433	
Goodness-of-fit on F^2	1.025	
Final R indices [I>2sigma(I)]	R1 = 0.0525, wR2 = 0.1398	
R indices (all data)	R1 = 0.0773, wR2 = 0.1575	
Extinction coefficient	n/a	
Largest diff. peak and hole	1.414 and -0.988 $e.Å^{-3}$	

Table S5. Crystal data and structure refinement for EuCu**L**.

Identification code	EuCu**L**	
Empirical formula	$C_{52}H_{56}Cl_3CuEuN_{10}O_{20}$	
Formula weight	1462.91	
Temperature	99.99(10) K	
Wavelength	1.54184 Å	
Crystal system	Orthorhombic	
Space group	Fdd2	
Unit cell dimensions	a = 32.0987(4) Å	□α = 90°.
	b = 19.3371(3) Å	□β = 90°.
	c = 18.1716(2) Å	□ γ = 90°.
Volume	11279.0(3) $Å^3$	
Z	8	
Density (calculated)	1.723 Mg/m^3	
Absorption coefficient	10.406 mm^{-1}	
F(000)	5928	
Crystal size	0.1 x 0.07 x 0.03 mm^3	
Theta range for data collection	3.611 to 66.599°.	
Index ranges	-26<=h<=38, -22<=k<=22, -21<=l<=21	
Reflections collected	12795	
Independent reflections	4461 [R(int) = 0.0252]	
Completeness to theta = 66.599°	99.7 %	
Absorption correction	Semi-empirical from equivalents	
Max. and min. transmission	1.00000 and 0.65245	
Refinement method	Full-matrix least-squares on F^2	
Data / restraints / parameters	4461 / 4 / 405	
Goodness-of-fit on F^2	0.890	
Final R indices [I>2sigma(I)]	R1 = 0.0284, wR2 = 0.0746	
R indices (all data)	R1 = 0.0288, wR2 = 0.0749	
Absolute structure parameter	0.149(3)	
Extinction coefficient	n/a	
Largest diff. peak and hole	0.627 and -0.645 $e.Å^{-3}$	

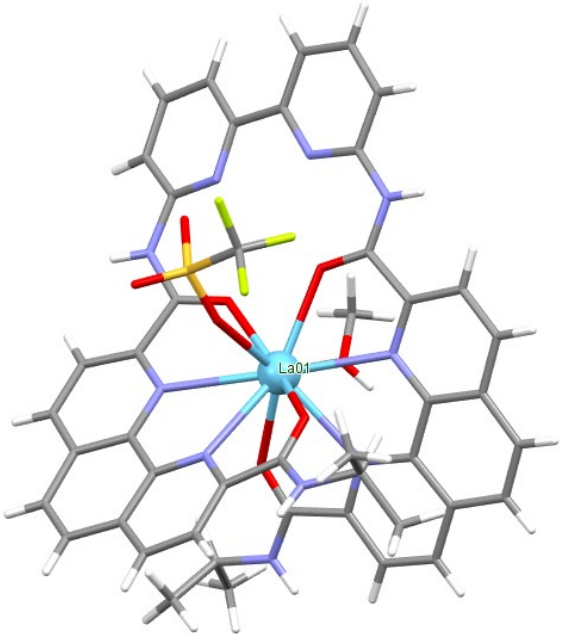

Figure S53. Crystal structure of La**L**.

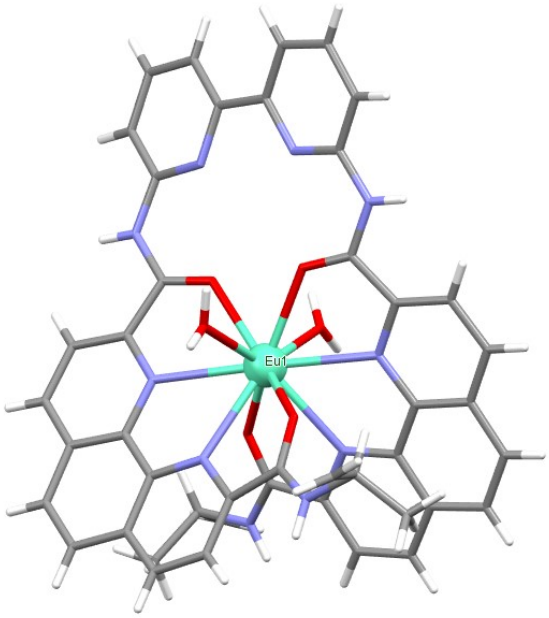

Figure S54. Crystal structure of Eu**L**.

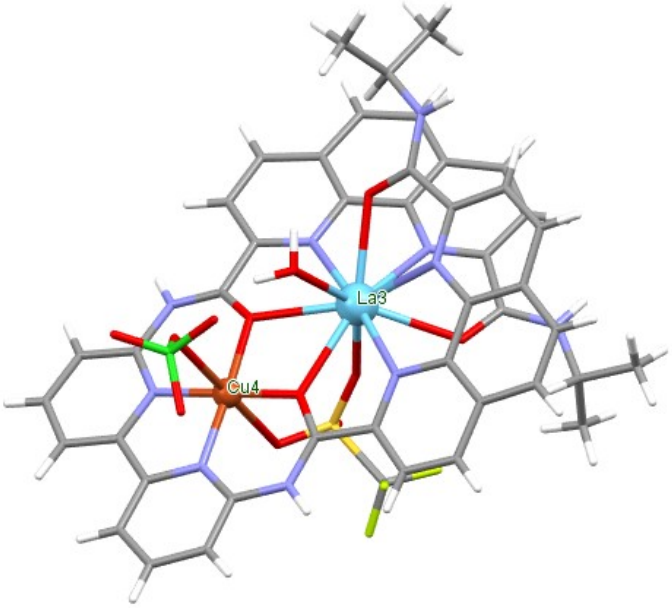

Figure S55. Crystal structure of LaCu**L**.

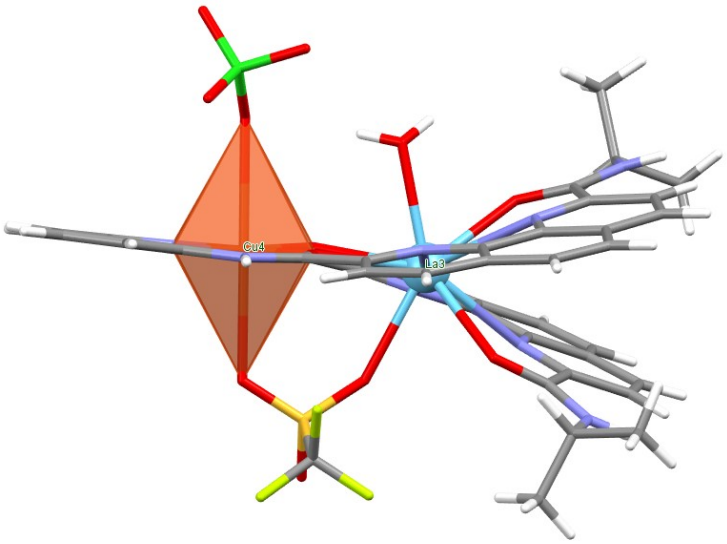

Figure S56. Crystal structure of LaCu**L** with polyhedral view of Cu^{2+} center.

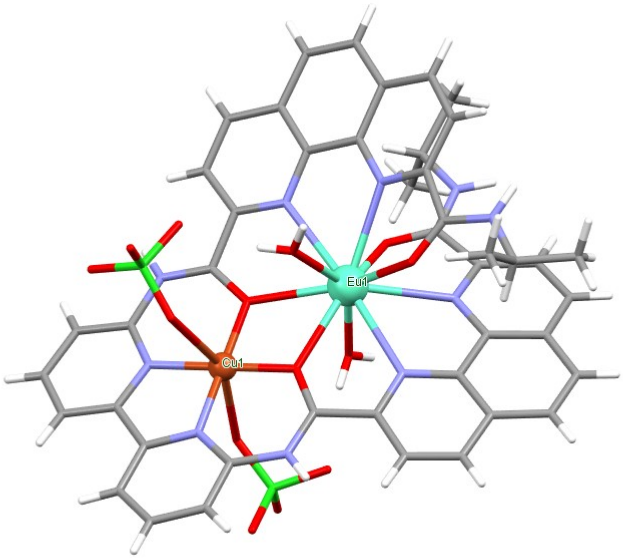

Figure S57. Crystal structure of EuCu**L**.

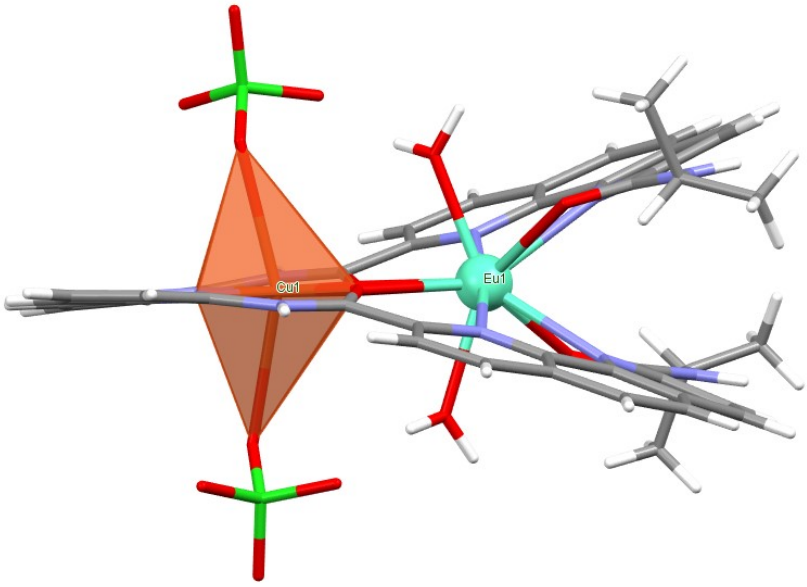

Figure S58. Crystal structure of EuCu**L** with polyhedral view of Cu^{2+} center.

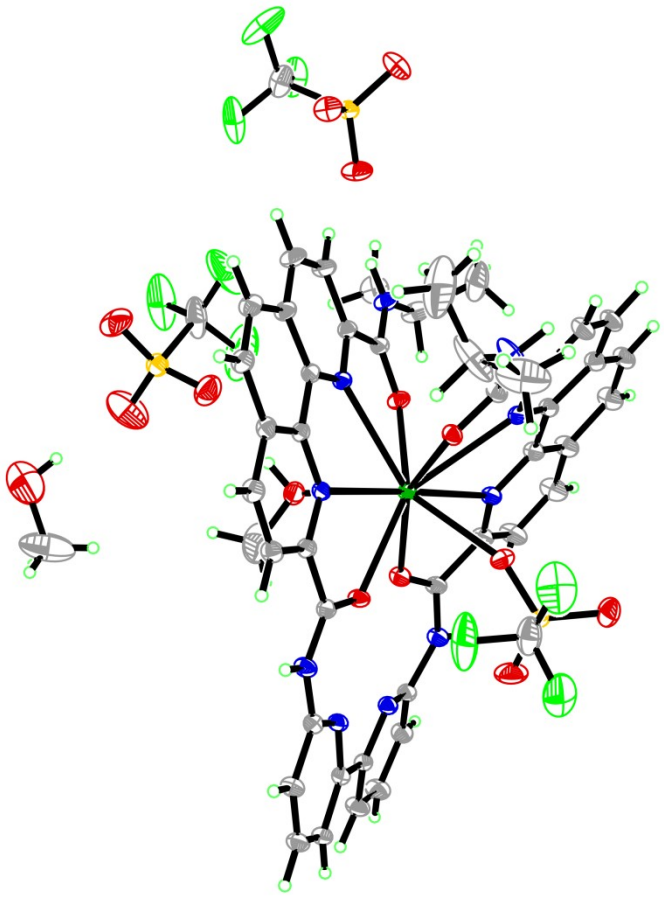

Figure S59. Ortep drawing of the asymmetry unit in the crystal structure of La**L** at 30 % probability level.

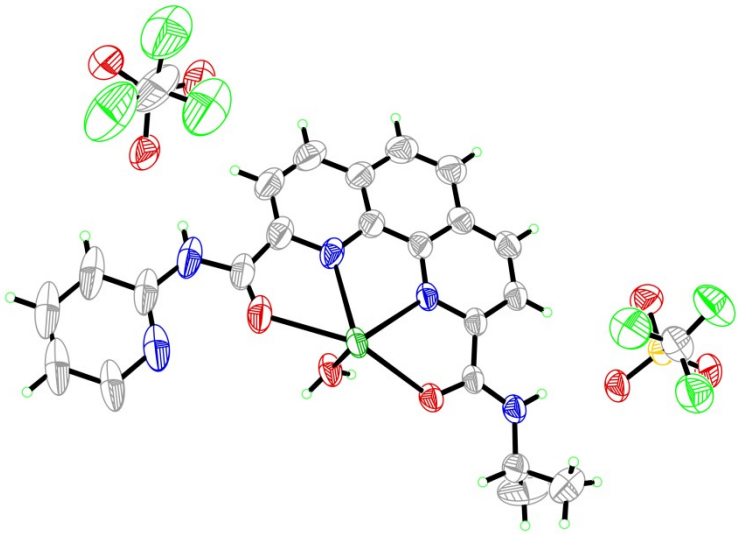

Figure S60. Ortep drawing of the asymmetry unit in the crystal structure of Eu**L** at 30 % probability level.

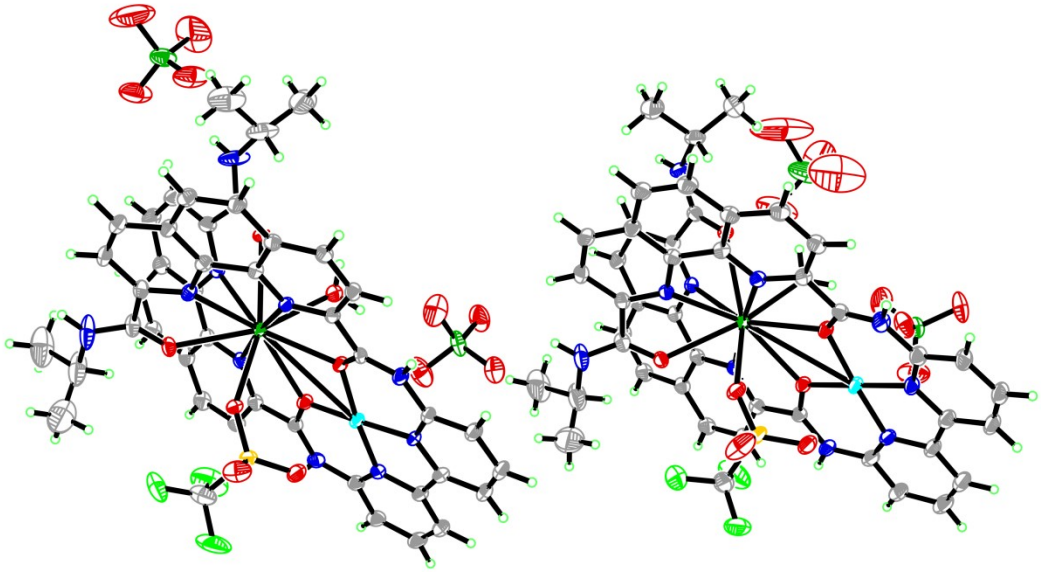

Figure S61. Ortep drawing of the asymmetry unit in the crystal structure of LaCu**L** **a**t 30 % probability level.

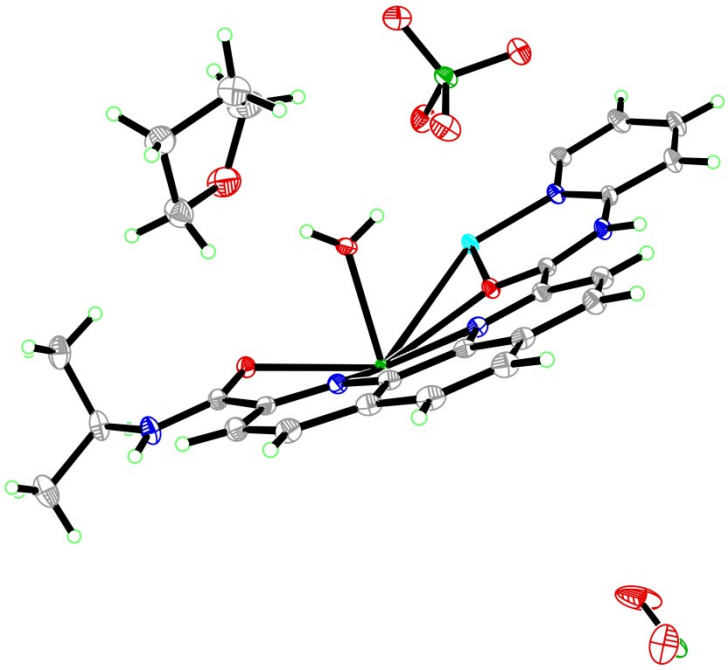

Figure S62. Ortep drawing of the asymmetry unit in the crystal structure of EuCu**L** at 30 % probability level.

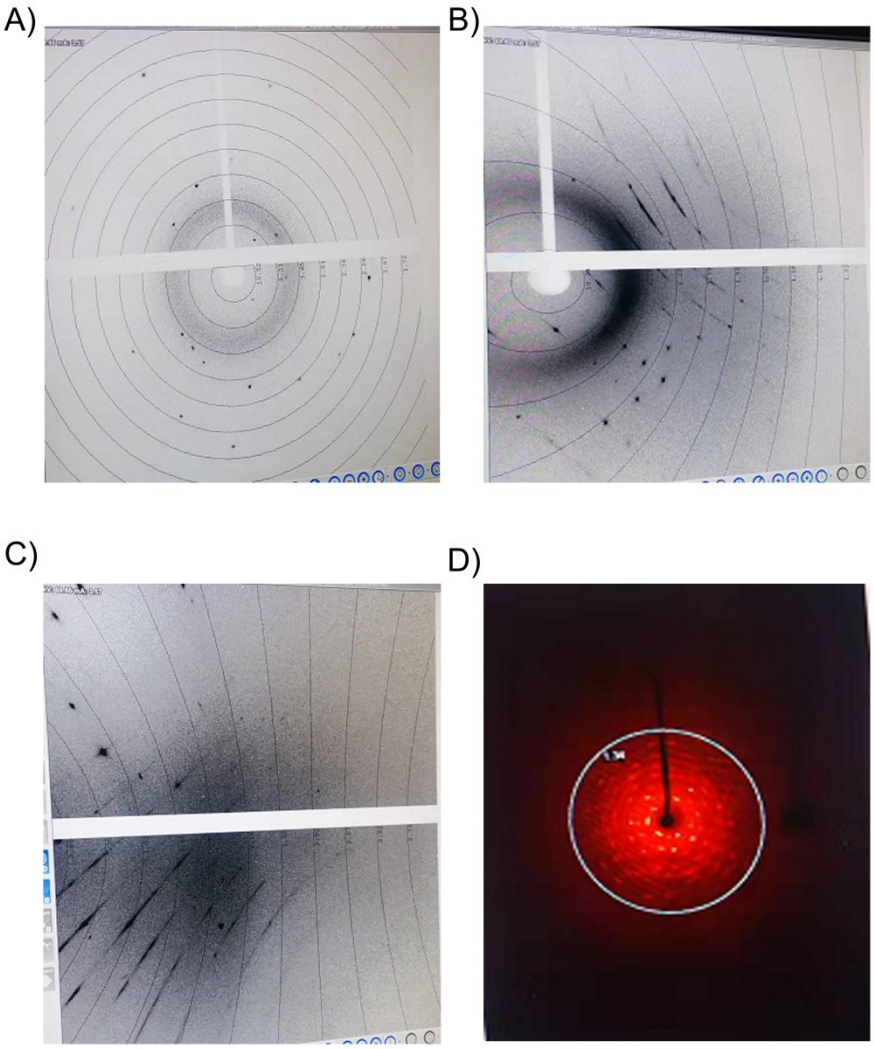

Figure S63. Photographs of Lu**L** crystals diffracted under X-ray after 1, 5 and 10 minutes respectively at room temperature (A- C) or 100 K (D)

8. Reference

[S1] R, S. K.; Kumar, S. K. A.; Vijayakrishna, K.; Sivaramakrishna, A.; Brahmmananda Rao, C. V. S.; Sivaraman, N.; Sahoo, S. K. *Inorg. Chem.* **2018,** *57*, 15270.

[S2] D. H. Wu, A.D. Chen, C. S. Johnson *J. Magn. Reson., Ser A,* **1995**, *115*, 260.

[S3] (a) Benesi, H. A.; Hildebrand, G. *J. Am. Chem. Soc.* **1949,** *71*, 2703; (b) Barra, M.; Bohne, C.; Scaiano, J. C. *J. Am. Chem. Soc.* **1990**, *112*, 8075.

[S4] Agilent Technologies, *CrysAlisPro* v. 1.171.36.28, **2013**.

[S5] APEX III, Data collection software (version 2017.3).

[S6]. Sheldrick, G. M., *Acta Crystallogr. Sect. A,* **2008**, *64*, 112.

[S7] Spek, A. L. Single-Crystal Structure Validation with the Program PLATON. *J. Appl. Crystallogr.* **2003**, *36*, 7.